SEDIMENTOLOGY the journal of the International Association of Sedimentologists

Sedimentology (2021) **68**, 1539–1579 doi: 10.1111/sed.12776

Bedforms and sedimentary structures related to supercritical flows in glacigenic settings

JÖRG LANG*, DANIEL P. LE HERON†, JAN H. VAN DEN BERG‡ and JUTTA WINSEMANN*

**Institut für Geologie, Leibniz Universität Hannover, Callinstraße 30, Hannover 30167, Germany (E-mail: winsemann@geowi.uni-hannover.de)*

†Department of Geodynamics and Sedimentology, University of Vienna, Althanstraße 14, Vienna 1090, Austria

‡Faculty of Earth Sciences, Utrecht University, Princetonlaan 8a, Utrecht 3584 CB, The Netherlands

Associate Editor – Dario Ventra

ABSTRACT

Upper-flow-regime bedforms, including upper-stage-plane beds, antidunes, chutes-and-pools and cyclic steps, are ubiquitous in glacigenic depositional environments characterized by abundant meltwater discharge and sediment supply. In this study, the depositional record of Froude near-critical and supercritical flows in glacigenic settings is reviewed, and similarities and differences between different depositional environments are discussed. Upper-flow-regime bedforms may occur in subglacial, subaerial and subaqueous environments, recording deposition by free-surface flows and submerged density flows. Although individual bedform types are generally not indicative of any specific depositional environment, some observed trends are similar to those documented in non-glacigenic settings. Important parameters for bedform evolution that differ between depositional environments include flow confinement, bed slope, aggradation rate and grain size. Cyclic-step deposits are more common in confined settings, like channels or incised valleys, or steep slopes of coarse-grained deltas. Antidune deposits prevail in unconfined settings and on more gentle slopes, like glacifluvial fans, sand-rich delta slopes or subaqueous (ice-contact) fans. At low aggradation rates, only the basal portions of bedforms are preserved, such as scour fills related to the hydraulic-jump zone of cyclic steps or antidune-wave breaking, which are common in glacifluvial systems and during glacial lake-outburst floods and (related) lake-level falls. Higher aggradation rates result in increased preservation potential, possibly leading to the preservation of complete bedforms. Such conditions are met in sediment-laden jökulhlaups and subaqueous proglacial environments characterized by expanding density flows. Coarser-grained sediment leads to steeper bedform profiles and highly scoured facies architectures, while finer-grained deposits display less steep bedform architectures. Such differences are in part related to stronger flows, faster settling of coarse clasts, and more rapid breaking of antidune waves or hydraulic-jump formation over hydraulically rough beds.

Keywords Antidune, cyclic step, chute-and-pool, glacifluvial delta, ice-contact fan, jökulhlaup.

INTRODUCTION

The role of upper-flow-regime processes for deposition in many clastic depositional environments is increasingly recognized. These bedforms are produced at high Froude numbers at near-critical and supercritical flow conditions and include upper-stage-plane beds, antidunes, chutes-and-pools and cyclic steps. The formation of different bedform types is controlled by the (densimetric) Froude number, grain size, sediment concentration and confinement of the formative flow (Van den Berg & Van Gelder, 1993, 1998; Alexander *et al.*, 2001; Kostic, 2011, 2014; Cartigny *et al.*, 2014; Fedele *et al.*, 2016). Upper-flow-regime bedforms have been documented mostly from alluvial (e.g. Blair, 1999; Fielding, 2006; Froude *et al.*, 2017; Carling & Leclair, 2019), coastal and shallow-marine (Nielsen *et al.*, 1988; Massari, 1996, 2017; Slootman *et al.*, 2016, 2018, 2019; Vaucher *et al.*, 2018; Di Celma *et al.*, 2020) and deep-marine deposits (Postma *et al.*, 2014; Covault *et al.*, 2017; Lang *et al.*, 2017a; Hage *et al.*, 2018; Ono & Plink-Björklund, 2018).

The formation and preservation of upper-flow-regime bedforms is generally thought to be favoured in settings with high rates of aggradation and rapidly decelerating flows. These conditions are commonly met in meltwater-dominated glacigenic depositional environments, which are characterized by abundant sediment supply and large spatial and temporal variations in flow strength and discharge (Marren, 2005; Cuffey & Paterson, 2010; Dowdeswell *et al.*, 2015), including rare high-magnitude events due to outbursts of stored meltwater (Duller *et al.*, 2008; Carling, 2013). Previous studies have documented different types of upper-flow-regime bedforms in successions from glacigenic depositional environments characterized by abundant meltwater and sediment supply (Brennand, 1994; Hirst *et al.*, 2002; Russell & Arnott, 2003; Kjær *et al.*, 2004; Hornung *et al.*, 2007; Duller *et al.*, 2008; Winsemann *et al.*, 2009, 2011, 2016, 2018; Girard *et al.*, 2012a,b, 2015; Lang & Winsemann, 2013; Pisarska-Jamroży & Zieliński, 2014; Dietrich *et al.*, 2016, 2017; Lang *et al.*, 2017b).

This study provides a review of the depositional record of upper-flow-regime bedforms in glacigenic depositional environments preserved in successions from Palaeozoic and Quaternary glacial episodes in Earth's history. The overall objective is to demonstrate that upper-flow-regime bedforms are formed under a broad variety of flow conditions in glacigenic environments, making the latter an ideal setting for the recognition and study of the stratigraphic signatures of supercritical flows. The study aims to: (i) summarize the controlling factors for bedform morphodynamics and the characteristic sedimentary facies in the different sub-environments of glacigenic deposition; (ii) discuss the specific conditions for the development of upper-flow-regime bedforms in glacigenic depositional settings; and (iii) point out the similarities and differences of deposits of upper-flow-regime bedforms to non-glacigenic depositional environments.

Morphodynamics of bedforms related to supercritical flows

Upper-flow-regime bedforms are known to occur within various sub-environments of glacigenic settings, including subglacial, glacifluvial, glacilacustrine and glacimarine environments (Fig. 1). The large variability in documented bedform scales relates to the very different magnitudes of the formative flows, ranging from shallow sheetfloods in glacifluvial systems (Pisarska-Jamroży & Zieliński, 2014) to deep density flows in glacilacustrine and glacimarine systems (Winsemann *et al.*, 2009, 2018; Hirst, 2012; Lang & Winsemann, 2013; Lang *et al.*, 2017b) and glacial lake-outburst floods (Carling *et al.*, 2009; Winsemann *et al.*, 2011, 2016).

To encompass the wide range of glacigenic depositional environments (Fig. 1) where Froude supercritical flows may occur, some terms used throughout this study need a definition. Subaerial depositional environments are settings characterized by processes related to subaerial runoff, i.e. free-surface or open-channel flows in hydrodynamic terms. The term open-channel flow, however, does not necessarily indicate channelization. Subaerial depositional environments characterized by flowing air (i.e. aeolian) are not considered here. Subaqueous depositional environments are settings characterized by gravity-driven density flows propagating at the base of an ambient water column. The density flows considered here generally have an excess density generated by the sediment load and is higher than the density of the ambient water mass (i.e. sediment-gravity flows). Examples for this group of density flows are low-density and high-density turbidity currents, hyperpycnal flows or underflows (Mulder & Alexander, 2001; Talling *et al.*, 2012).

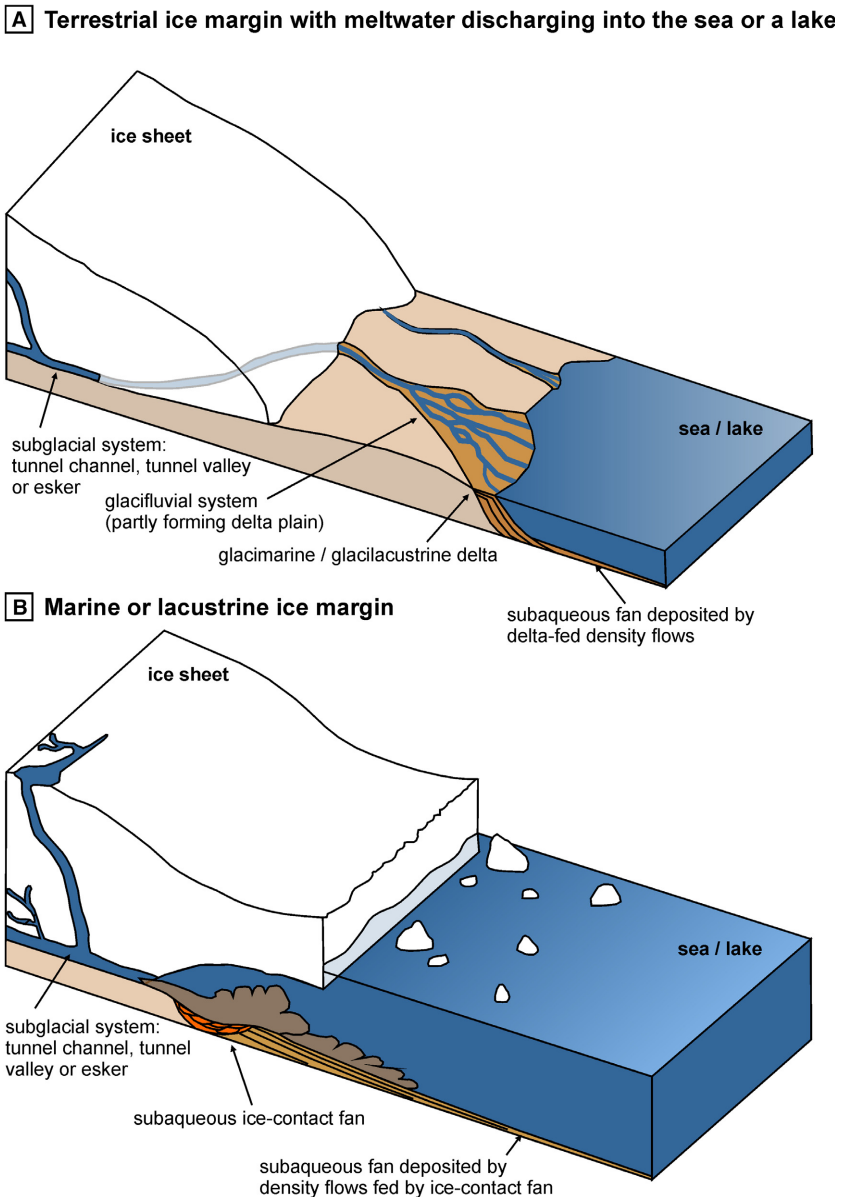

Fig. 1. Schematic sketch of the occurrence of the different glacigenic depositional environments (modified after Cuffey & Paterson, 2010; Chu, 2014). (A) Terrestrial ice margin. (B) Glacimarine or glacilacustrine ice margin.

The most commonly described bedforms related to near-critical and supercritical flows are antidunes, chutes-and-pools and cyclic steps (Fig. 2) (Van den Berg & Van Gelder, 1993, 1998; Alexander *et al.*, 2001; Kostic, 2011, 2014; Cartigny *et al.*, 2014; Fedele *et al.*, 2016). Supercritical flows are characterized by the dominance of inertial over gravitational forces and are defined by a Froude number larger than unity. For free-surface flows (also termed open-channel flows), the Froude number (Fr) is given by $Fr = \bar{U}/\sqrt{(g'h)}$, where $\bar{U}$ is the depth-averaged flow velocity, h is the flow depth and g is the acceleration by gravity. For density flows, the densimetric Froude number Fr′ is given by $Fr' = \bar{U}/\sqrt{(g'h)}$, where g′ is the reduced acceleration by gravity with $g' = g(\rho_f\text{-}\rho_w)/\rho_f$, where ρ_f is the density of the flow and ρ_w is the density of the ambient water. Supercritical flows over mobile sediment beds are characterized by in-phase relationships between the morphology of the sediment-flow interface and disturbances of the upper surface of the flow, which in density flows is represented by a density interface internal to the flow (Hand, 1974; Cartigny *et al.*, 2014; Postma & Cartigny, 2014; Fedele *et al.*, 2016). The formation of upper-flow-regime bedforms requires a free upper flow interface and is therefore suppressed in full pipe-flow conditions (Banerjee & McDonald, 1975).

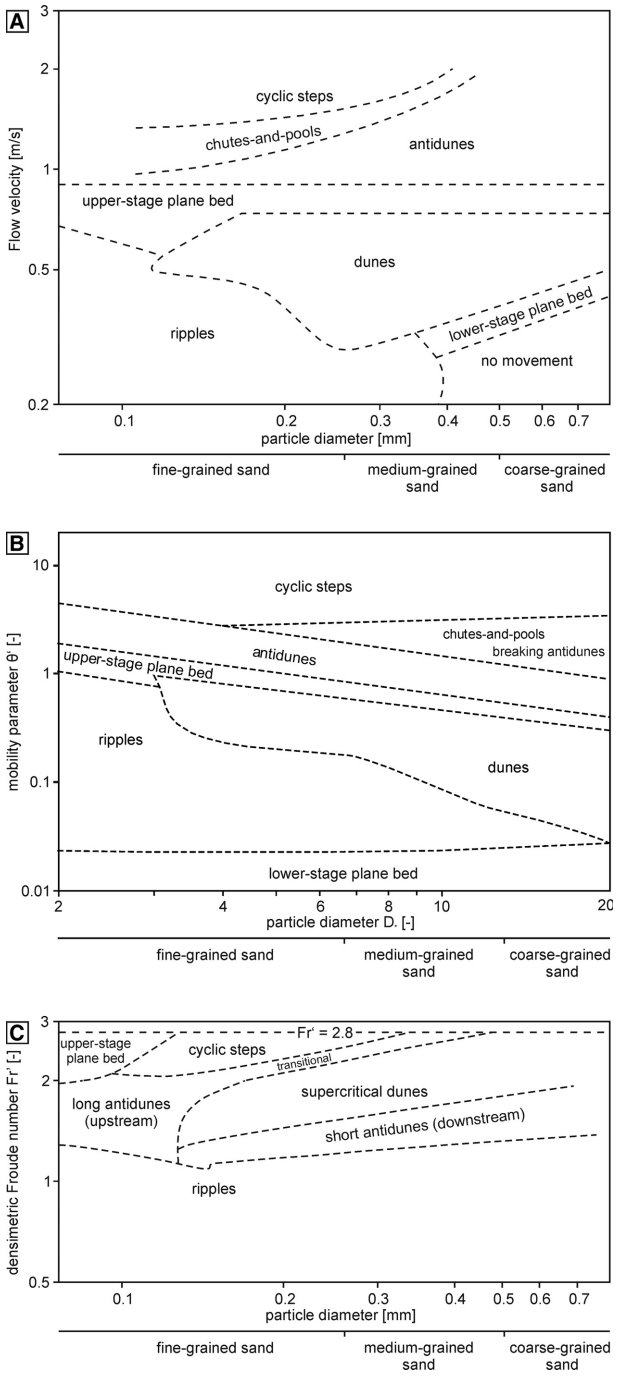

Fig. 2. Bedform stability diagrams. (A) Stability fields of free-surface flows plotted for particle diameter versus flow velocity for a flow depth of 0.06 to 0.1 m (modified from Southard & Boguchwal, 1990; Cartigny *et al.*, 2014). (B) Stability fields of free-surface flows plotted for the dimensionless particle diameter versus dimensionless mobility parameter (modified from Van den Berg & Van Gelder, 1998; Cartigny *et al.*, 2014). (C) Stability fields of submerged density flows plotted for particle diameter versus. densimetric Froude number (modified from Fedele *et al.*, 2016).

Depending on (densimetric) Froude number and grain size various types of bedforms develop. For equilibrium conditions in free surface flows the bedforms are well-known from flume experiments and observations in rivers, and their occurrence can be predicted in bedform stability diagrams (Fig. 2A and B). For density flows this is not the case, due to the difficulty to produce stable sediment-density flows in flumes over time periods long enough to create an equilibrium with the evolving bedforms. Cartigny & Postma (2016) presented a series of stability diagrams for bedforms produced by 10 m thick sediment density flows with increasing basal sediment concentration. These authors assumed that the stability fields are basically the same as for free-surface flows, except for a plane-bed stage produced by traction carpets in high-density turbidity currents. Fedele *et al.* (2016) published a new stability diagram based on a very large number of flume experiments with saline density flows (Fig. 2C). Because the flows in these experiments were not charged with suspended sediment, the diagram may only represent the bed morphodynamics of dilute density flows. The upper limit for upper-flow-regime bedform existence is $Fr' = 2.8$ (Fig. 2C) (Mastbergen & Van Den Berg, 2003). Above this threshold Kelvin–Helmholtz billows developed at the density flow interface with the overlying less dense fluid reach the bed, resulting in sudden dilution and thickening of the density flow by mixing with the overlying fluid, which in turn causes a reduction of the densimetric Froude number.

Consequently, the densimetric Froude number cannot rise much above this threshold (Mastbergen & Van Den Berg, 2003). Upper-flow-regime bedforms are probably more common in density flow deposits, where supercritical conditions are more easily attained than in free-surface flows and high rates of aggradation result in greater preservation potential (Hand, 1974; Covault *et al.*, 2017). However, these observations might be biased by the strong focus of recent studies on density flows and their deposits. The expression of upper-flow-regime bedforms within the depositional record is also strongly controlled by the rate of aggradation and grain-size distribution, which may lead to very different sedimentary structures (Cartigny *et al.*, 2014; Ono *et al.*, 2021). In addition, reduced aggradation rates may result in a low variability of sedimentary structures (Cartigny *et al.*, 2014), and hence reduce the ability to distinguish between bedforms.

Experiments by Cartigny *et al.* (2014) have shown that transitions between the stability fields of antidunes, chutes-and-pools and cyclic steps are poorly defined in the grain size versus Froude number parameter space, probably due to strong flow–particle interactions. Bedform stability fields and their transitions could be better defined by means of the dimensionless particle diameter and the mobility parameter (Fig. 2C) (Cartigny *et al.*, 2014). The dimensionless particle diameter (D^*) is given by $D^* = D_{50}\ ((\rho_s - \rho_f)g/\rho_f\ \nu)^{1/3}$, where D_{50} is the median grain size of the bed material, ρ_s is the density of the sediment particles and ν is the kinematic viscosity of the flow. The dimensionless mobility parameter (Θ^*) is given by $\Theta^* = \rho_f\ \bar{U}^2/(\rho_s - \rho_f)(C')^2\ D_{50}$, where C' is the grain-size related Chezy coefficient. The advantage of using the dimensionless particle diameter and the mobility parameter for bedform stability diagrams (Fig. 2B) is that no shift is expected in the boundaries of the stability fields in the diagram in case of changing the temperature, gravity or fluid density (Van Den Berg & Van Gelder, 1993, 1998).

Upper-flow-regime bedforms can be classified as stable versus unstable bedform types (Cartigny *et al.*, 2014; Slootman & Cartigny, 2019). Bedforms may exist as stable patterns as shown in flume experiments with steady flows, while in nature flows are commonly highly unsteady (Alexander *et al.*, 2001; Cartigny *et al.*, 2014; Fedele *et al.*, 2016). A classic example of unsteady and non-uniform flow is the plane bed – stationary antidunes – breaking antidunes cycle described by Middleton (1965). Upper-flow-regime bedforms should always be considered as inherently unstable under natural conditions and can only be regarded as stable for a short interval of time. However, an exception to this is given by cyclic steps, which once formed can remain active and propagate upstream for very long times, if the flow and sediment supply are sustained.

Antidunes

Antidunes are characterized by in-phase trains of surface waves that may be stationary or migrate upflow or downflow, resulting in the formation of a range of bedforms with variable morphodynamics. If the wave steepness (wave height/wavelength) exceeds a critical value (0.142 in open-channel flows), wave breaking may occur at the flow surface, triggering the cyclic destruction and regeneration of underlying antidune bedforms (Kennedy, 1963; Middleton, 1965; Cartigny *et al.*, 2014). The wave steepness of antidunes along the upper interfaces of density flows is generally lower than at the upper interface of free-surface flows, leading to the formation of more stable wave trains less susceptible to wave breaking (Fedele *et al.*, 2016). Antidunes are classified according to their migration direction (stationary, upstream-migrating or downstream-migrating), wavelength and non-breaking (stable antidunes) versus breaking (unstable antidunes) dynamics (Gilbert, 1914; Kennedy, 1963; Alexander *et al.*, 2001; Cartigny *et al.*, 2014; Fedele *et al.*, 2016), leading to a range of sedimentary structures. Tabular beds with trains of backsets, subhorizontal, convex-up or sinusoidal stratification or low-angle cross-stratification point to non-breaking antidunes. Lenticular beds with backsets, low-angle foresets or concave-up concentric infill indicate breaking antidunes (Alexander *et al.*, 2001; Fielding, 2006; Duller *et al.*, 2008; Lang & Winsemann, 2013; Cartigny *et al.*, 2014). Stationary non-breaking antidunes may deposit sinusoidal strata, matching the in-phase relation between the flow and the bedforms (Middleton, 1965; Brennand, 1994; Duller *et al.*, 2008; Lang & Winsemann, 2013). Upstream-migration or downstream-migration of non-breaking antidunes causes an upflow or downflow offset of the wave crests, respectively (Fielding, 2006; Lang & Winsemann, 2013). If antidune migration becomes more pronounced the sedimentary structures are characterized by backsets or foresets (Van den Berg & Lang, this issue; Ito, 2010; Cartigny *et al.*, 2014; Fedele *et al.*, 2016; Lang *et al.*, 2017a,b). Furthermore, the expression of antidune bedforms within deposits is also strongly controlled by the rate of aggradation at the original sediment–water interface, where generally reduced aggradation rates may result in low variability of structures (Cartigny *et al.*, 2014), and hence a reduced ability to distinguish the variety of antidunes.

Chutes-and-pools

The morphodynamics of chutes-and-pools are characterized by irregularly spaced supercritical flow reaches (the chute) and subcritical flow reaches (the pool) separated by a hydraulic jump. The hydraulic jumps migrate erratically and may spontaneously form and dissipate (Alexander *et al.*, 2001; Cartigny *et al.*, 2014). However, the exact nature of chute-and-pool bedforms is still debated, and it is possible that these mobile-bed configurations simply reflect

transient, pronounced flow instabilities at the transition between antidunes and cyclic steps at intermediate Froude numbers (Fig. 2A and B) (Cartigny *et al.*, 2014; Slootman & Cartigny, 2019). Deposits of chutes-and-pools typically consist of scours infilled by steeply dipping backsets occasionally accompanied by gently dipping foresets, as well as concentric scour fills. These scour fills are commonly associated with local evidence for antidune deposits formed in the supercritical reach of the formative flow (Hand, 1974; Alexander *et al.*, 2001; Fielding, 2006; Lang & Winsemann, 2013; Cartigny *et al.*, 2014; Postma *et al.*, 2021). Such isolated scour fills are also referred to as deposits of isolated or localized hydraulic jumps (Russell & Arnott, 2003; Duller *et al.*, 2008; Lang *et al.*, 2017b), avoiding explicit reference to possible chute-and-pool bedforms, which might not have been fully preserved. Isolated hydraulic jumps may form also in response to changing flow conditions forced by local slope breaks, for example at the toe of deltas (Winsemann *et al.*, 2007b; Massari, 2017; Postma *et al.*, 2020), at the base of steep barrier spits or beach ridges (Nielsen *et al.*, 1988; Di Celma *et al.*, 2020), or at large flow obstacles, such as stranded ice blocks during a jökulhlaup (Russell & Knudsen, 2002; Burke *et al.*, 2010a; Herget *et al.*, 2013).

Cyclic steps

Cyclic steps are formed at high Froude numbers by flows characterized by alternating reaches with supercritical and subcritical conditions bounded by hydraulic jumps that migrate upflow at a constant distance, defining the wavelength of an individual cyclic step. Cyclic-step morphodynamics are dominated by deposition downflow of the hydraulic jumps and erosion upflow of the hydraulic jumps, typically leading to the formation of asymmetrical bedforms (Cartigny *et al.*, 2011, 2014; Ventra *et al.*, 2015; Fedele *et al.*, 2016; Slootman & Cartigny, 2019). Cyclic-step deposits are commonly characterized by laterally stacked scours filled by massive or diffusely graded/stratified sediment and gently dipping backsets (Postma *et al.*, 2009, 2014; Cartigny *et al.*, 2014; Postma & Cartigny, 2014). Due to the similarity of depositional processes in the hydraulic-jump zone, the distinction between cyclic-step and chute-and-pool deposits remains challenging. Criteria for the recognition of cyclic-step deposits include the predominance of asymmetrical backset cross-stratified scour fills and the lateral stacking of scour fills produced by the steady migration of the hydraulic jumps (Cartigny *et al.*, 2014; Lang *et al.*, 2017a; Postma *et al.*, 2020). Superimposed antidunes may form in the supercritical flow reach on the stoss sides of cyclic steps (Van den Berg & Lang, this issue; Kostic, 2014; Zhong *et al.*, 2015; Lang *et al.*, 2017a). If cyclic steps and antidunes form in the same train, the wavelength of the cyclic steps is typically one order of magnitude larger than the wavelength of the associated antidunes (Kostic, 2014).

Further upper-flow-regime bedforms

Further bedforms developed at near-critical to supercritical flow stages are: (i) upper-stage-plane beds; (ii) humpback dunes; and (iii) supercritical dunes (Fig. 2). Upper-stage-plane beds are formed by bedload sheets and very low-amplitude bed waves, and are characterized by thin (commonly millimetre-scale) planar-parallel stratification in the resulting deposits (Allen, 1984; Paola *et al.*, 1989; Best & Bridge, 1992). In density flows, upper-stage-plane beds have been attributed to deposits of dilute turbidity currents ('$T_{B\text{-}1}$'; Talling *et al.*, 2012) and have been reproduced in flume experiments (Fedele *et al.*, 2016; Koller *et al.*, 2019). In contrast to free-surface flows, where they are produced at near-critical Froude numbers, plane beds represent conditions of relatively high densimetric Froude numbers in density flows. Notwithstanding this fundamental difference, flume experiments show the same bedload sheets as in free-surface flows, suggesting similar depositional processes (Fedele *et al.*, 2016; Koller *et al.*, 2019). Humpback dunes display sigmoidal foreset cross-stratification, with best preserved examples showing a clear differentiation between topset, foreset and bottomset laminae. They are generally considered as bedforms transitional between subcritical dunes and antidunes, forming commonly under high aggradation rates (Saunderson & Lockett, 1983; Chakraborty & Bose, 1992; Fielding, 2006; Lang & Winsemann, 2013; Winsemann *et al.*, 2018). Humpback dunes have originally been described from fluvial environments, where they are commonly flattened and washed-out when upper-stage-plane beds or antidunes develop under increasing flow velocity (Saunderson & Lockett, 1983; Fielding, 2006). However, humpback dunes can also develop at subcritical Froude numbers in deep fluvial and estuarine channels for conditions of fine-grained sand and high bed-grain mobility (Røe, 1987; Martinius & Van den Berg, 2011). In

this case, the formation of sigmoidal cross-stratification can be considered as an initial stage in the transition from dunes to upper-plane-bed regime not forced by a high Froude number, but by the suppression of turbulence by a high near-bed vertical gradient in suspended bed material (Bridge & Best, 1988).

Supercritical dunes are asymmetrical, downstream-migrating bedforms observed in supercritical density flows. Internally, they are characterized by sigmoidal or tangential foreset cross-stratification (Fedele *et al.*, 2016; Lang *et al.*, 2017a). In flume experiments, supercritical dunes display clear flow-separation on the lee sides, lack an in-phase relationship with the flow and form at higher densimetric Froude numbers than downstream-migrating antidunes (Fedele *et al.*, 2016). Subcritical dunes did not form in the experiments of Fedele *et al.* (2016) because the bed-shear stress necessary for dune formation was only attained in supercritical flows.

However, distinguishing between deposits of humpback dunes, supercritical dunes and downstream-migrating antidunes might be nearly impossible as the characteristic sedimentary structure of these three bedform types is sigmoidal foreset cross-stratification (Saunderson & Lockett, 1983; Fielding, 2006; Lang & Winsemann, 2013; Fedele *et al.*, 2016; Lang *et al.*, 2017a,b; Winsemann *et al.*, 2018). The issue is further complicated because sigmoidal cross-stratification may also relate to subcritical (climbing) dunes under high rates of aggradation (Ghienne *et al.*, 2010; Winsemann *et al.*, 2011) and isolated hydraulic-jump bars (Macdonald *et al.*, 2009, 2013).

THE DEPOSITIONAL RECORD OF GLACIGENIC UPPER-FLOW-REGIME BEDFORMS

Deposits of upper-flow-regime bedforms have been documented from a variety of glacigenic depositional environments within Palaeozoic and Quaternary successions (Table 1). Direct observations of upper-flow-regime bedforms in modern glacigenic settings include antidune trains on glacifluvial fans (Gustavson, 1974) and cyclic steps in supraglacial meltwater streams (Izumi *et al.*, 2017). The best example of cyclic steps in a modern submarine setting are from the subaqueous slope of the sand-rich glacifluvial Squamish River delta in western Canada, where bedform morphodynamics, flow triggers and the resulting stratigraphy have been studied in detail from direct observations (Hughes Clarke, 2016; Stacey & Hill, 2016; Hizzett *et al.*, 2018; Hage *et al.*, 2018, 2019; Stacey *et al.*, 2019; Vendettouli *et al.*, 2019). Deposits of antidunes and chutes-and-pools are known from modern jökulhlaup deposits in Alaska and Iceland, where the depositional record can be compared with direct observations and estimations of the flood discharge (Burke *et al.*, 2008, 2010a,b; Duller *et al.*, 2008, 2015).

Pleistocene glacigenic successions occur worldwide in high-latitude and high-altitude settings and are generally very well studied. Detailed documentation of upper-flow-regime bedforms, which were mostly produced by meltwater floods in the vicinity of the ice margin, come from successions related to the Fennoscandian (e.g. Hornung *et al.*, 2007; Winsemann *et al.*, 2009, 2011, 2018; Lang & Winsemann, 2013; Pisarska-Jamroży & Zieliński, 2014; Lang *et al.*, 2017b) and British–Irish ice sheets (e.g. Lee *et al.*, 2015; Leszczynska *et al.*, 2017, 2018) in Europe and the Laurentide Ice Sheet in North America (e.g. Brennand, 1994; Russell & Arnott, 2003; Johnsen & Brennand, 2004; Dietrich *et al.*, 2016, 2017).

The Late Palaeozoic Ice Age (Fielding *et al.*, 2010; Montañez & Poulsen, 2013) resulted in the expansion of ice sheets across Gondwana, with a general diachronous trend charting the drift of South Gondwana over the South Pole. A rich archive of glacigenic deposits and associated sand-rich outwash complexes is recorded for example from Devonian basins in Bolivia (Bache *et al.*, 2012), Late Carboniferous to Permian basins of Argentina, Brazil and Uruguay (Vesely *et al.*, 2015; Aquino *et al.*, 2016; Alonso-Muruaga *et al.*, 2018; Assine *et al.*, 2018), roughly coeval successions in South Africa (Dietrich & Hofmann, 2019) and Ethiopia (Bussert, 2014), and Permian deposits in Oman (Martin *et al.*, 2012) and Australia (Fielding *et al.*, 2010). With the sole exception of the eastern Karoo Basin, South Africa (Dietrich *et al.*, 2019), there is no specific interpretation of upper-flow-regime bedforms in Late Palaeozoic glacigenic strata. The reason for this is probably neither lack of evidence nor failed preservation, but failed recognition.

Successions related to the Late Ordovician (Hirnantian) glaciations of Gondwana are widespread and well documented from North Africa and the Arabian Peninsula (Le Heron *et al.*,

Table 1. Overview of well documented field examples of upper-flow-regime bedforms in glacigenic deposits.

Bedform	Grain size	Geometry	Sedimentary structures[a]	Dimensions[b]: length (l); width (w); thickness (d); aspect ratio (l/d); wavelength (λ); amplitude (y); wave steepness (y/λ); cross-set dip (α)	Location; Age; Database	References
Subglacial (esker)						
Antidunes	Sand to gravel	Tabular	Sinusoidal stratification	d: 1–3 m; λ: 4–10 m; y: 1–3 m; y/λ: 0.25–0.3; α: 10°	Wales (UK); Pleistocene; outcrop	Lee *et al.* (2015)
Antidunes	Pebble to cobble gravel	Tabular	Sinusoidal stratification	λ: 12 m; y: 3 m; y/λ: 0.25	Alaska (USA) and Iceland; Holocene; georadar	Burke *et al.* (2008, 2010b)
Glacifluvial						
Chutes-and-pools	Pebbly sand	Lenticular	Scours filled by concave-up backsets	l: 0.3–1.3 m; d: 0.04–0.3 m; d/l: 0.2; α: 12–34°	Northern Germany; Pleistocene; outcrop	This study
Antidunes	Pebbly sand	Tabular	Low-angle cross-stratification and subhorizontal stratification	d: 0.05–0.2 m; α: 5–10°	Northern Germany; Pleistocene; outcrop	This study
Antidunes	Pebbly sand	Tabular	Low-angle cross-stratification	d: 0.05 m; α: <10°	Iceland; Holocene; outcrop	Kjær *et al.* (2004)
Upper-stage-plane beds	Pebbly sand	Tabular	Planar-parallel stratification	d: 0.3 m	Iceland; Holocene; outcrop	Kjær *et al.* (2004)
Upper-stage-plane beds	Granule to cobble gravel	Tabular	Planar-parallel stratification	d: 0.8–1.2 m	Poland; Pleistocene; outcrop	Pisarska-Jamroży & Zieliński (2014)
Upper-stage-plane beds	Coarse-grained sand	Tabular	Planar-parallel stratification	d: 0.1–1.0 m	Poland; Pleistocene; outcrop	Pisarska-Jamroży & Zieliński (2014)

Table 1. (continued)

Bedform	Grain size	Geometry	Sedimentary structures[a]	Dimensions[b]: length (l); width (w); thickness (d); aspect ratio (l/d); wavelength (λ); amplitude (y); wave steepness (y/λ); cross-set dip (α)	Location; Age; Database	References
Jökulhlaups/glacial lake-outburst floods						
Cyclic steps	Pebbly sand	Lenticular	*In-flow:* Scours with thin massive basal layer and gently-dipping concave-up backsets. *Across-flow:* Scours with concave-up concentric infills or subhorizontal stratification	l: 2–13 m; d: 0.1–0.4 m; l/d: 0.04; α: 5–10°	Northern Germany; Pleistocene; outcrop	Lang & Winsemann (2013)
Cyclic steps or antidunes	?	Tabular	Sinusoidal stratification; shorter wavelength features are associated with isolated foreset-filled scours	l: 350 m; d: 10 m; λ: 60–90 m; y: 3.8–5.0 m; y/λ: 0.06	Northern Germany; Pleistocene; outcrop and georadar	Winsemann *et al.* (2018); Kostic *et al.* (2019)
Chutes-and-pools	Interbedded gravel and sand	Lenticular	Sigmoidal backsets	l: 7 m; d: 3 m; d/l: 0.4; α: 30°	Switzerland; Pleistocene; outcrop	Fiore *et al.* (2002)
Chutes-and-pools	Scoria granule gravel	Lenticular	Infill of regular-based scours; base concordant concave-up stratification; onlap on base of scour	l: up to 60 m; d: 3–4 m; d/l: 0.09–0.11; λ: 10 m; y: 0.2 m; y/λ: 0.02	Iceland; Holocene; outcrop	Duller *et al.* (2008)
Local hydraulic jump formed at isolated trough or obstacle	Scoria granule gravel	Lenticular	Infill of scours with steep upflow margin; convex-up stratification; onlap on scour base and upflow margin	l: 13 m; d: 3 m; d/l: 0.11	Iceland; Holocene; outcrop	Duller *et al.* (2008)
Local hydraulic jump formed at obstacle	Cobble to boulder gravel	Lenticular	*In-flow:* Scour fill with foresets (lee side) and backsets (stoss side). *Across-flow:* Convex-up scour fill	l: 40–70 m; w: 15–20 m; d: 3–7 m; d/l: 0.1–0.7	Iceland; Holocene; outcrop and georadar	Burke *et al.* (2010a)
Antidunes (net-erosional)	Pebble gravel	Waveforms	Waveforms are eroded into diamicton and draped by up to 2.5 m thick gravel	λ: 300 m; y: >10 m; y/λ: 0.03	Altai Mountains (Russia); Pleistocene; outcrop	Carling *et al.* (2002, 2009)

Table 1. (continued)

Bedform	Grain size	Geometry	Sedimentary structures[a]	Dimensions[b]: length (l); width (w); thickness (d); aspect ratio (l/d); wavelength (λ); amplitude (y); wave steepness (y/λ); cross-set dip (α)	Location; Age; Database	References
Antidunes (net-erosional)	Gravel	Waveforms	Backsets	d: 1.5 m; λ: 100–230 m; y: 6–14 m; y/λ: 0.06; α: 15–35°	British Columbia (Canada); Pleistocene; outcrop and georadar	Johnsen & Brennand (2004)
Non-breaking antidunes	Scoria granule gravel	Tabular or lenticular	Concave-up stratification above a gently inclined concave-up basal surface	l: 45 m; d: 0.5–2.0 m; d/l: 0.01–0.09; λ: 24–96 m; y: 0.3–1.3 m; y/λ: 0.02; α: <10°	Iceland; Holocene; outcrop	Duller *et al.* (2008)
Antidunes	Pebbly sandstone	Tabular	Sinusoidal stratification and subhorizontal stratification	d: 10–20 m; λ: 100 m; y: 5 m; y/λ: 0.05	Murzuq Basin (Libya); Upper Ordovician; outcrop	Girard *et al.* (2015)
Subaqueous ice-contact fans (glacilacustrine/ glacimarine)						
Chutes-and-pools	Fine to medium-grained sand	Lenticular	Diffusely graded or cross-stratified scour fills	l: 20 m; d: 3; d/l: 0.15	Ontario (Canada); Pleistocene; outcrop	Russell *et al.* (2007)
Chutes-and-pools	Granule to cobble gravel	Lenticular	Scours filled by concave-up backsets	l: 1.7–4.6 m; w: 2–13 m; d: 0.35–0.9; d/l: 0.11–0.26; α: 12–44°	Northern Germany; Pleistocene; outcrop and georadar	Lang *et al.* (2017b)
Chutes-and-pools	Pebbly sand	Lenticular	*In-flow:* Scours filled by steeply dipping concave-up or planar backsets. *Across-flow:* Concave-up concentric scour fills	l: 0.4–0.8 m; d: 0.2–0.3 m; d/l: 0.4; α: 10–20°	Northern Germany; Pleistocene; outcrop	Lang & Winsemann (2013)
Chutes-and-pools	Pebbly sand	Lenticular	Scours filled by planar or concave-up backsets	l: 0.4–13 m; w: 0.5–1.5; d: 0.08–1.5 m; d/l: 0.1–0.2; α: 10–20°	Northern Germany; Pleistocene; outcrop and georadar	Lang *et al.* (2017b)

Table 1. (continued)

Bedform	Grain size	Geometry	Sedimentary structures[a]	Dimensions[b]: length (l); width (w); thickness (d); aspect ratio (l/d); wavelength (λ); amplitude (y); wave steepness (y/λ); cross-set dip (α)	Location; Age; Database	References
Local hydraulic jump	Pebbly sand	Lenticular	Massive or diffusely graded infill of steep-walled scours	d: 3 m	Ontario (Canada); Pleistocene; outcrop	Russell & Arnott (2003)
Local hydraulic jump	Granule to boulder gravel	Lenticular	Massive, normally graded or planar cross-stratified infill of scours	l: up to 25 m; d: 1–3 m; l/d: 0.04–0.12; α: 10–30°	Northern Germany; Pleistocene; outcrop and georadar	Hornung *et al.* (2007) Winsemann *et al.* (2009)
Breaking antidunes	Pebble to cobble gravel	Tabular	Pebble to sandy gravel couplets with planar stratification; local gravel clusters	l: 8–10 m; d: 0.5–2.0 m; d/l: 0.06–0.2	Ontario (Canada); Pleistocene; outcrop	Russell & Arnott (2003)
Breaking antidunes	Pebbly sand	Tabular or lenticular	*In-flow:* Subhorizontal stratification or low-angle cross-stratification; scours with convex-up or concave-up foresets or backsets. *Across-flow:* Concave-up concentric scour fills or subhorizontal stratification	l: 0.5–16 m; w: 2–13 m; d: 0.3–1.5 m; d/l: 0.09–0.6 m; α: 5–15°	Northern Germany; Pleistocene; outcrop and georadar	Lang *et al.* (2017b)
Breaking antidunes	Granule to cobble gravel	Lenticular or tabular	Subhorizontal stratification or low-angle cross-stratification	l: 1.9–9.5 m; d: 0.2–1.5 m; d/l: 0.1; α: <10°	Northern Germany; Pleistocene; outcrop and georadar	Lang *et al.* (2017b)
Non-breaking antidunes	Pebble to cobble gravel	Tabular	In-phase waveforms	λ: 12 m; y: 0.5 m; y/λ: 0.04	Ontario (Canada); Pleistocene; outcrop	Brennand (1994)
Non-breaking antidunes	Pebbly sand	Tabular	In-phase waveforms; internal diffuse grading	λ: 5–20 m; y: 0.25–1.25 m; y/λ: 0.05	Ontario (Canada); Pleistocene; outcrop	Brennand (1994)
Non-breaking antidunes	Medium-grained sand	Tabular	Low-angle cross-stratification	l: 8–10 m; d: 0.4–1.5 m	Ontario (Canada); Pleistocene; outcrop	Russell & Arnott (2003)

Table 1. (continued)

Bedform	Grain size	Geometry	Sedimentary structures[a]	Dimensions[b]: length (l); width (w); thickness (d); aspect ratio (l/d); wavelength (λ); amplitude (y); wave steepness (y/λ); cross-set dip (α)	Location; Age; Database	References
Non-breaking antidunes	Sand and pebbly sand	Tabular	*In-flow:* Sinusoidal stratification. *Across-flow:* Concave-up or convex-up lenticular and subhorizontally undulating geometries	l: 7–40 m; w: 3–13 m; d: 0.5–1.2 m; λ: 1.2–40 m; y: 0.1–0.7 m; y/λ: 0.02–0.05; α: <10°	Northern Germany; Pleistocene; outcrop and georadar	Lang & Winsemann (2013); Lang *et al.* (2017b)
Delta slopes (glacilacustrine/glacimarine)						
Cyclic steps[c]	Mud, <5% sand	Waveforms	Downslope asymmetrical sinusoidal stratification	l: 3000 m; w: 2000 m; d: 60 m; d/l: 0.02; λ: 16–600 m; 0.1–8.6 m; y/λ: 0.02; α: 3.8–7.7° (stoss side) 1.7–2.9° (lee side)	Yukon (Canada); Holocene; sub-bottom profiles	Gilbert & Crookshanks (2009)
Cyclic steps	Pebbly sand	Lenticular	Scours with gently dipping concave-up backsets	d: 1–3 m; λ: 10–20 m; y: 1–3 m; y/λ: 0.1	Quebec (Canada); Pleistocene; outcrop	Dietrich *et al.* (2016)
Cyclic steps	Medium to coarse-grained sand	Waveforms	Massive or subhorizontally stratified	d: 1–5 m; λ: 10–20 m	Quebec (Canada); Pleistocene; outcrop	Dietrich *et al.* (2017)
Cyclic steps	Pebbly sand	Lenticular	*In-flow:* Scours with concave-up or sigmoidal backsets; basal scour fill may be massive or normally graded. *Across-flow:* Concave-up or convex-up concentric scour-fills	l: 0.7–7 m; w: 1–5 m; d: 0.08–1.6 m; d/l: 0.01–0.1; α: 5–23°	Northern Germany; Pleistocene; outcrop and georadar	Lang *et al.* (2017b); Winsemann *et al.* (2018)
Cyclic steps	Pebbly sand to pebble gravel	Lenticular	Scours with gently dipping concave-up backsets	l: 0.5–1.0 m; d: 0.1–0.3 m; d/l: 0.2–0.3	Northern Germany; Pleistocene; outcrop and georadar	Winsemann *et al.* (2011, 2018); Kostic *et al.* (2019)

Table 1. (continued)

Bedform	Grain size	Geometry	Sedimentary structures[a]	Dimensions[b]: length (l); width (w); thickness (d); aspect ratio (l/d); wavelength (λ); amplitude (y); wave steepness (y/λ); cross-set dip (α)	Location; Age; Database	References
Antidunes	Pebbly sand	Lenticular	Sinusoidal stratification and subhorizontal stratification	d: 0.2–5.0 m; λ: 3 m	Quebec (Canada); Pleistocene; outcrop	Dietrich *et al.*, 2017)
Breaking antidunes	Pebbly sand	Tabular	Low-angle cross-stratification	l: 0.5–4.0 m; d: 0.05–0.7 m; α: 5–15°		
Non-breaking antidunes	Medium to coarse-grained sandstone	Tabular or waveforms	Horizontal to subhorizontal stratification within undulating bedforms	d: 1–10 m; λ: 40 m; y: 0.5–2.0 m; y/λ: 0.01–0.05	Murzuq Basin (Libya); Upper Ordovician; outcrop	Girard *et al.* (2012b)
Non-breaking antidunes	Medium-grained sand	Tabular	Sinusoidal stratification	d: <1 m; λ: 1 m; y: 0.1 m; y/λ: 0.1 m	Murzuq Basin (Libya); Upper Ordovician; outcrop	Girard *et al.* (2012b)
Glacimarine density flows						
Non-breaking antidunes	Fine-grained sandstone	Tabular	Sinusoidal stratification	d: 2–3 m; λ: 2.0–2.5 m; y: 0.1–0.25 m; y/λ: 0.05–0.1 m	Illizi Basin (Algeria); Upper Ordovician; outcrop	Hirst *et al.* (2002)
Non-breaking antidunes	Fine-grained sandstone	Tabular	Sinusoidal stratification	d: 0.5–5.0 m; λ: 1.5–3.5 m; y: 0.1–0.25 m; y/λ: 0.07 m	Murzuq Basin (Algeria); Upper Ordovician; outcrop	Hirst (2012)

[a]Sedimentary structures are generally described in flow parallel direction only. If across flow descriptions are available, this is highlighted.
[b]Length refers to flow parallel dimension; width refers to flow normal dimension. Only the available dimensions are provided.
[c]The bedforms are referred to as 'sediment waves' in the original publication (Gilbert & Crookshanks, 2009). However, the inferred sedimentary process exactly matches cyclic steps.

2009). The dominantly glacifluvial and glacimarine successions indicate depositional environments with abundant meltwater and supply of sand-grade sediment (Le Heron *et al.*, 2009; Bataller *et al.*, 2019). These conditions should favour the formation and preservation of upper-flow-regime bedforms, which indeed have been documented by a range of studies (Hirst *et al.*, 2002; Le Heron *et al.*, 2010, 2013, 2015; Hirst, 2012; Lang *et al.*, 2012; Girard *et al.*, 2012a,b, 2015; Moreau & Joubert, 2016).

Unlike Pleistocene and Palaeozoic records, no upper-flow-regime bedforms have been described from the Neoproterozoic record. Excellent exposures of diamictite successions are known globally (Arnaud *et al.*, 2011). The issue appears to be that the successions are either dominated by thick, stacked diamictites (Le Heron *et al.*, 2014) or alternatively by fine-grained turbidites intercalated with chemical precipitates (Lechte *et al.*, 2018). Although upper-flow-regime bedforms are known from deposits of fine-grained low-density turbidity currents (Fedele *et al.*, 2016; Lang *et al.*, 2017a; Onishi *et al.*, 2018), they have so far not been reported from the abundant slope and deep-marine deposits, which prevail as a general rule in the Cryogenian glacial record (Busfield & Le Heron, 2016; Spence *et al.*, 2016). Ice-proximal successions comparable to the North Gondwanan record of the Hirnantian glaciation were yet not described, possibly due to a preservational bias in glacimarine rift basins, favouring the preservation of diamictites over meltwater deposits (Eyles & Januszczak, 2004; Eyles, 2008).

UPPER-FLOW-REGIME BEDFORMS IN DIFFERENT GLACIGENIC DEPOSITIONAL ENVIRONMENTS

Subglacial environments

Subglacial meltwater deposits form in subglacial meltwater conduits and may be preserved in eskers or as the infills of tunnel channels and tunnel valleys (Fig. 1; Table 1). Eskers are typically deposited in meltwater conduits incised upward into the ice, while tunnel channels and tunnel valleys are incised into the substratum. Tunnel channels represent subglacial conduits adjusted to the magnitude of the (bankfull) meltwater discharge, while tunnel valleys are larger-scale features cut during multiple episodes of erosion and deposition. Both eskers and tunnel-valley fills may include ice-marginal and other non-subglacial deposits, and may include non-glacigenic deposits formed after ice-sheet retreat (Banerjee & McDonald, 1975; Brennand, 1994; Russell *et al.*, 2003; Kehew *et al.*, 2012; Lang *et al.*, 2012; Janszen *et al.*, 2013; Ahokangas & Mäkinen, 2014; Steinmetz *et al.*, 2015).

Antidune deposits have been described from successions inferred to have been deposited in subglacial environments, although their formation should be suppressed under full pipe-flow conditions in subglacial conduits (Banerjee & McDonald, 1975). The occurrence of these deposits in subglacial environments can be explained by: (i) the occurrence of high-density, internally stratified underflows within a full conduit; (ii) non-full pipe-flow conditions; and (iii) flows expanding into subglacial cavities or lakes (Brennand, 1994; Brennand & Shaw, 1996; Fisher *et al.*, 2003; Russell *et al.*, 2003; Burke *et al.*, 2008, 2010b; Lee *et al.*, 2015). At the ice margins there is commonly a transition between subglacial tunnel-valley fills and eskers, respectively, and glacifluvial systems at terrestrial ice margins or subaqueous ice-contact fans, if the ice margin terminates in a water body (Gorrell & Shaw, 1991; Brennand, 1994; Russell *et al.*, 2003; Deschamps *et al.*, 2013; Ahokangas & Mäkinen, 2014).

Burke *et al.* (2008, 2010b) documented antidune strata in the basal part of modern esker deposits in Alaska and Iceland, with wavelengths of up to 12 m and amplitudes of up to 3 m. The eskers are interpreted to have formed during jökulhlaups in subglacial or englacial conduits close to the ice margin (Burke *et al.*, 2008, 2010b). Fiore *et al.* (2002) observed chute-and-pool deposits in Pleistocene esker deposits in Switzerland. The deposits consist of sigmoidal gravelly and sandy backsets that infill up to 3 m deep and more than 7 m wide troughs. Chutes-and-pools are interpreted to have formed in wider segments of subglacial conduits during jökulhlaup conditions (Fiore *et al.*, 2002).

Subaerial depositional environments

Sedimentary structures related to upper-flow-regime bedforms have commonly been described from subaerial meltwater deposits (Fig. 1A; Table 1). The observed sedimentary structures and bedforms are similar to those observed in non-glacigenic, high-energy, commonly braided fluvial systems (Alexander & Fielding, 1997; Fielding, 2006; Froude *et al.*, 2017; Carling & Leclair, 2019) and alluvial fans (Blair, 1999). Fielding (2006) proposed 'upper-flow-regime

sheets, lenses and scours fills' ('UFR') as a possible architectural element in fluvial deposits supplementing the widely applied architectural-element scheme of Miall (1985). Upper-flow-regime bedforms are considered as potentially indicative of fluvial sedimentation under strongly seasonal climate, with pronounced variability and discharge peakedness (Alexander & Fielding, 1997; Fielding, 2006; Froude *et al.*, 2017; Carling & Leclair, 2019; Wang & Plink-Björklund, 2020). These conditions are met also in glacifluvial systems, where meltwater discharge is subject to strong seasonal fluctuations (Marren, 2005; Cuffey & Paterson, 2010). Even more extreme discharge events in glacifluvial systems are represented by glacial lake-outburst floods or jökulhlaups caused by the release of water stored in proglacial, subglacial or supraglacial lakes. Such cataclysmic events contribute in a large measure to the accumulation of ice-proximal glacifluvial deposits (Pisarska-Jamroży & Zieliński, 2014) and may aggrade thick successions related to supercritical flows (Duller *et al.*, 2008; Lang & Winsemann, 2013; Winsemann *et al.*, 2016).

Glacifluvial deposits

Glacifluvial systems are formed by subaerial meltwater streams, which are generally characterized by braided channel networks (Fig. 1A) (Zielinski & van Loon, 2002, 2003; Blažauskas *et al.*, 2007; Pisarska-Jamroży & Zieliński, 2014). The sedimentology and geomorphology of glacifluvial systems are controlled by the scale of the system, the meltwater and sediment supply, the local hydraulic gradients and lateral confinement. Steep glacifluvial systems commonly form small-scale fan shaped sediment bodies, referred to as *sandar* (singular: *sandur*), which may resemble alluvial fans. Gently sloping glacifluvial systems form larger-scale braidplains, which may merge into ice-marginal trunk rivers (Zielinski & van Loon, 2002, 2003; Blažauskas *et al.*, 2007) or feed into glacifluvial deltas (Slomka & Hartman, 2019).

Deposits of upper-stage-plane beds and antidunes are interpreted to form in shallow braided channels and unconfined sheetfloods during high discharge events in the melt season (Figs 3 and 4) (Zielinski & van Loon, 2002, 2003; Krzyszkowski, 2002; Kjær *et al.*, 2004; Pisarska-Jamroży & Zieliński, 2014). Kjær *et al.* (2004) described gravelly and sandy antidune deposits from an Icelandic sandur. Gravelly antidune deposits display subhorizontal and backset cross-stratification, while sandy antidune deposits display low-angle cross-stratification and are associated with sandy upper-stage-plane beds (Kjær *et al.*, 2004). Pisarska-Jamroży & Zieliński (2014) described several sedimentary facies related to supercritical flows from Pleistocene glacifluvial deposits in Poland. Massive clast-supported gravel is interpreted as representing rapid sedimentation from highly sediment-laden supercritical flows during peak-flood conditions. Horizontally stratified gravel and sand are deposited as upper-stage-plane beds by waning supercritical flows. Low-angle gravelly or sandy foreset cross-stratification points to the flattening of dunes at the transition from subcritical to supercritical flow conditions (Pisarska-Jamroży & Zieliński, 2014). Typical vertical successions pass from planar or low-angle cross-stratified gravel via horizontally stratified gravel into horizontally stratified sand, indicating the formation of longitudinal or transverse bars. Bar vertical accretion decreases the local flow depth and allows for the formation of upper-stage-plane beds (Pisarska-Jamroży & Zieliński, 2014).

Deposits of glacial lake-outburst floods and jökulhlaups. Glacial lake-outburst floods or jökulhlaups are cataclysmic drainage events due to the release of water stored in proglacial, subglacial or supraglacial lakes. The largest glacial lake-outburst events relate to the drainage of ice-dammed lakes along the margins of continental ice-sheets (Baker, 1973; Herget, 2005; Carrivick, 2006; Alho *et al.*, 2010; Carling, 2013; Margold *et al.*, 2018; Lang *et al.*, 2019; Panin *et al.*, 2020). Erosion and deposition by such floods have an enormous geomorphological impact due to the breaching of drainage divides and the re-routing of drainage systems (Baker, 1973; Mangerud *et al.*, 2004; Gupta *et al.*, 2007, 2017; Lang *et al.*, 2019; Panin *et al.*, 2020). Flow conditions during glacial lake-outburst floods are dominantly subcritical, due to the great flow depths. Supercritical flow conditions will commonly be attained due to local flow constrictions and shallow flows over valley margins or substratum obstacles (Carling *et al.*, 2009; Alho *et al.*, 2010; Bohorquez *et al.*, 2016; Winsemann *et al.*, 2016; Lang *et al.*, 2019; Hansen *et al.*, 2020).

Supercritical flows in outburst flood-related successions may form both net-erosional and net-depositional bedforms (Table 1). Net-erosional waveform structures of antidune origin incised during a major glacial lake-outburst flood were documented by Carling *et al.* (2002,

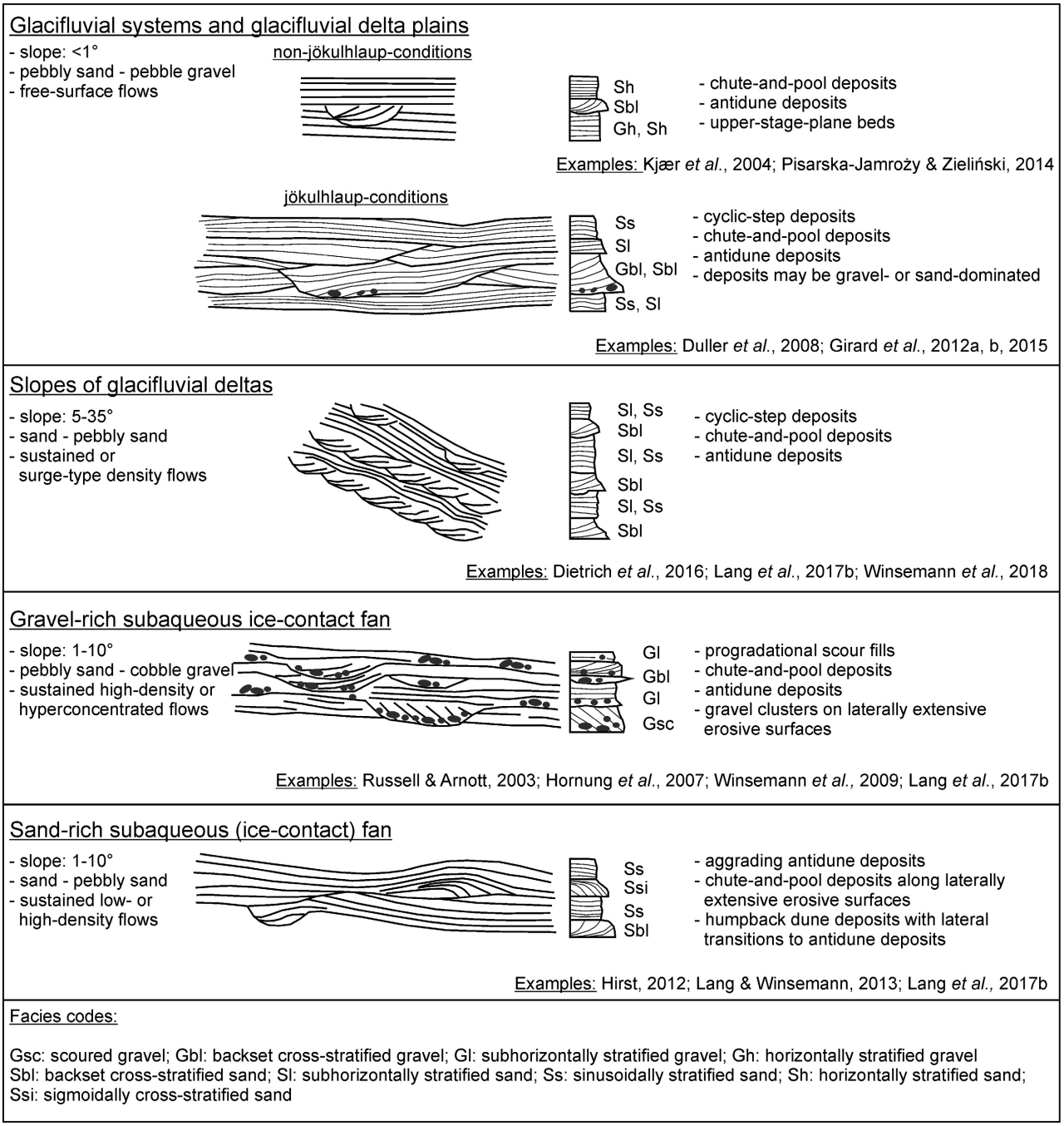

Fig. 3. Summary of characteristic features, depositional architectures and facies successions of deposits of upper-flow-regime bedforms in the different glacigenic depositional environments.

2009). In plan-view, the waveforms are straight crested with wavelengths of *ca* 300 m and amplitudes of up to 20 m. The waveforms are incised into diamicton. The formation of the antidune bed-waves is attributed to flow thinning in the lee of an obstacle (Carling *et al.*, 2002, 2009). Johnsen & Brennand (2004) documented slightly asymmetrical antidune waveforms of similar scale (wavelength 100 to 230 m, amplitude 6 to 14 m) on a glacifluvial delta plain truncated during a lake-drainage event. The preservation of up to 1.5 m thick backset cross-stratified gravel on the stoss-sides of the waveforms suggests a transition from

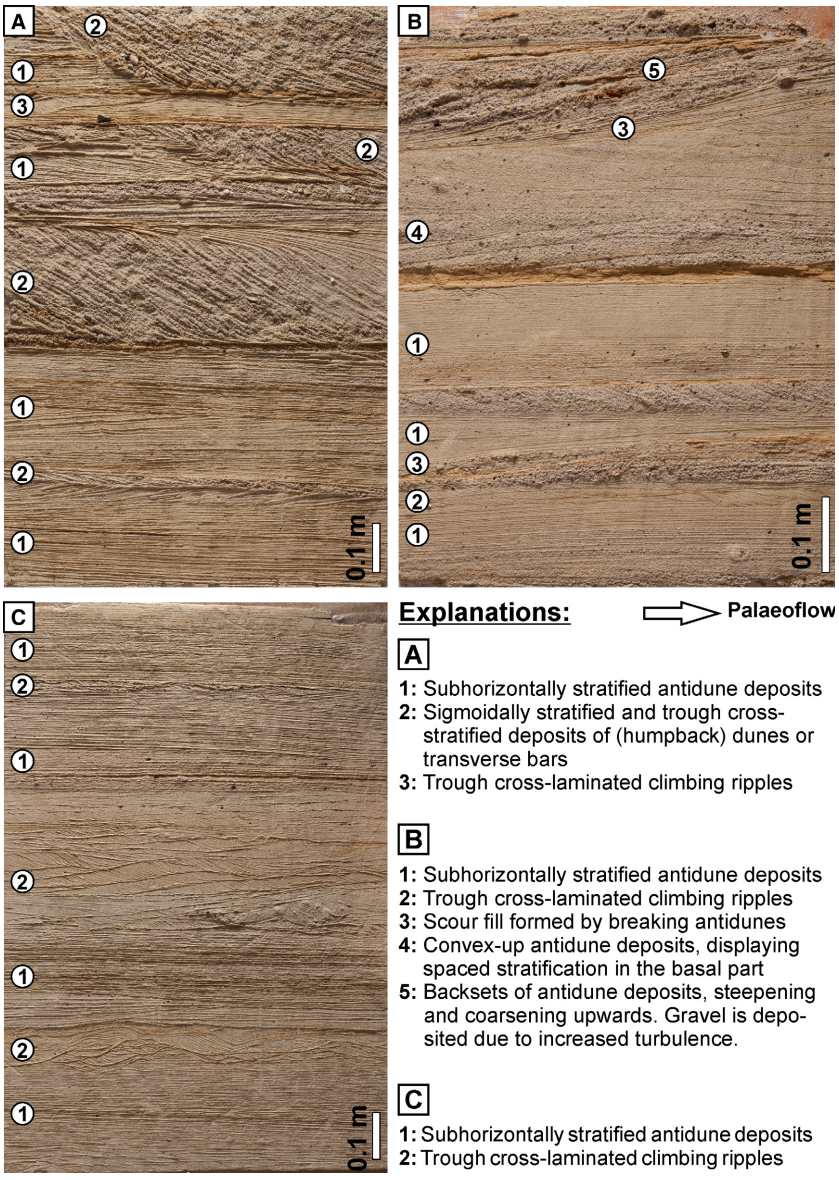

Fig. 4. Photographs of lacquer peels of upper-flow-regime bedforms in glacifluvial deposits (Werpeloh, northern Germany; Middle Pleistocene). The palaeoflow direction is approximately from the left in all peels.

degradational to aggradational conditions (Johnsen & Brennand, 2004; Carling *et al.*, 2009).

Deposits of cyclic steps, chutes-and-pools and antidunes have been documented from successions related to glacial lake-outburst floods and jökulhlaups (Figs 3, 5 and 6) (Duller *et al.*, 2008; Burke *et al.*, 2010a,b; Winsemann *et al.*, 2011; Lang & Winsemann, 2013; Le Heron *et al.*, 2013; Girard *et al.*, 2015; Winsemann *et al.*, 2016; Hansen *et al.*, 2020). Successions related to supercritical flows accumulated in the lee of glacitectonic ridges by a Pleistocene glacial lake-outburst flood were studied by Lang & Winsemann (2013) and Winsemann *et al.* (2016). An up to 15 m thick succession of pebbly sand, passing upward from cyclic-step and chute-and-pool deposits to deposits of antidunes, humpback dunes and three-dimensional dunes (Fig. 5A), was deposited within a channel incised by flows spilling over a glacitectonic ridge (Lang & Winsemann, 2013). Cyclic-step deposits are characterized by laterally and vertically amalgamated scour fills (length 2 to 13 m, depth 0.1 to 0.4 m) that contain low-angle (5 to 10°) backsets (Fig. 5A). Chute-and-pool deposits comprise amalgamated scour fills, which are 0.4 to 0.8 m long, 0.2 to 0.3 m deep and contain steeply dipping (10 to 20°) backsets. Deposits of chutes-and-pools are associated with antidune deposits that are characterized by up to 2.5 m

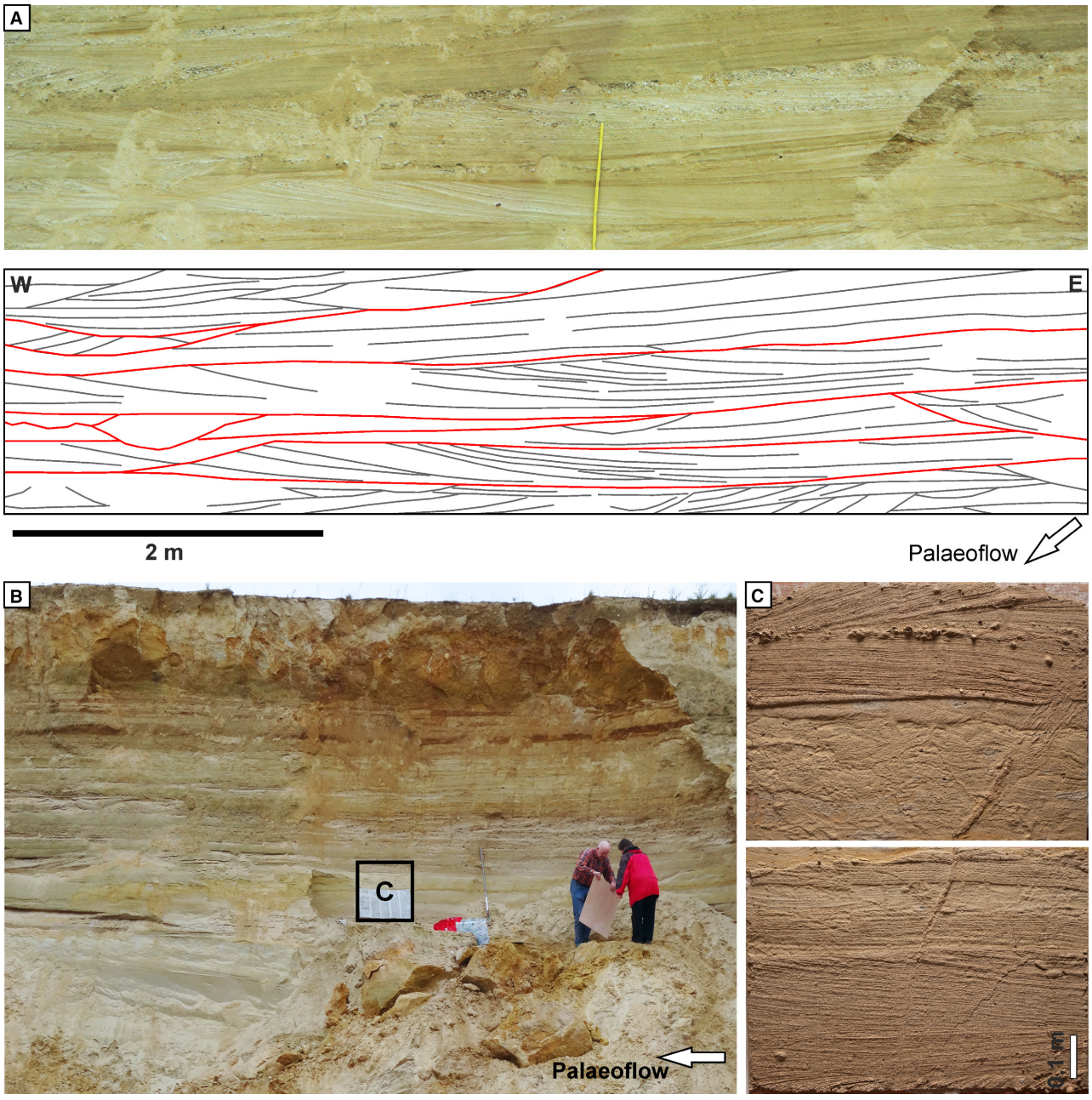

Fig. 5. Upper-flow-regime bedforms in deposits related to glacial lake-outburst floods. (A) Deposits of cyclic steps, comprising elongate scours filled by gently dipping backsets. The cyclic steps incised a channel when a glacial lake-outburst flood spilled over the Reichswald glacitectonic ridge (northern Germany; Middle Pleistocene; modified from Lang & Winsemann, 2013). (B) Overview of a succession formed in the lee of the Bönninghardt glacitectonic ridge during a glacial lake-outburst flood (northern Germany; Middle Pleistocene). The succession is dominated by low-angle cross-stratified antidune deposits and unconformably overlain by till. (C) Lacquer peel from the glacial lake-outburst flood deposits (location is indicated on Fig. 3B). Note the opposing dip directions of low-angle cross-sets deposited by antidunes. The water-escape pipe and the intense soft-sediment deformation in the central part point to elevated pore-water pressure due to rapid sedimentation.

thick tabular beds of low-angle cross-stratified and subhorizontally stratified pebbly sand (Fig. 5A). The variety of facies is interpreted as representing a single flood event, which dissected the glacitectonic ridge and subsequently accumulated a vertical facies succession related

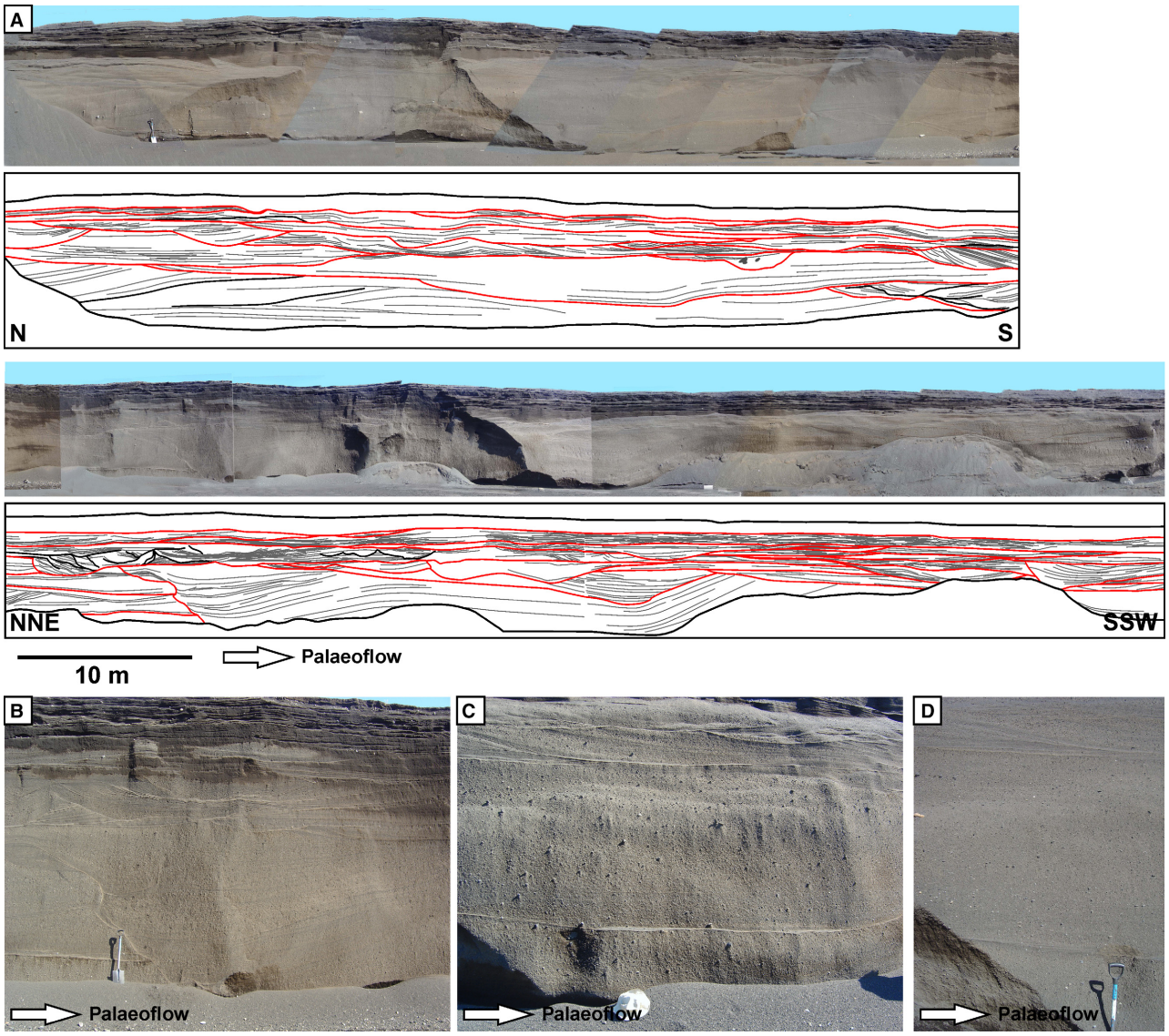

Fig. 6. Upper-flow-regime bedforms formed during a jökulhlaup (Mýrdalssandur, Iceland; Holocene). All photographs by courtesy of R. Duller. (A) Interpreted 'photo panel' of the jökulhlaup deposits. The succession comprises laterally and vertically stacked deposits of antidunes and chutes-and-pools (modified from Duller *et al.*, 2008). (B) Detail of a steep-walled scour margin interpreted as chute-and-pool deposit. Shovel for scale is *ca* 1 m. (C) Detail of the antidune deposits. The diffusely stratified to almost structureless sediment relates to the homogeneity of the scoria gravel and the rapid sedimentation from concentrated flows. Hat for scale is *ca* 45 cm (modified from Duller *et al.*, 2008). (D) Detail of the antidune deposits, showing an almost structureless *ca*. 1.5 m thick bed. Shovel handle for scale is *ca* 75 cm.

to waning flow conditions (Lang & Winsemann, 2013). Deposits of more unconfined, overspilling floodwaters were described by Winsemann *et al.* (2016) from a denudated glacitectonic ridge (Fig. 5B and C). The up to 10 m thick tabular succession comprises subhorizontally stratified and low-angle cross-stratified medium-grained sand to pebbly sand, indicating probable deposition by antidunes. Isolated scour fills may point to the occurrence of chutes-and-pools. The antidune deposits are associated with deposits of 3D dunes and climbing ripples, pointing to pulsating discharge conditions with rapidly changing flow velocity and depth (Winsemann *et al.*, 2016).

Duller *et al.* (2008) presented a detailed architectural analysis of Holocene volcaniclastic jökulhlaup deposits from an Icelandic sandur,

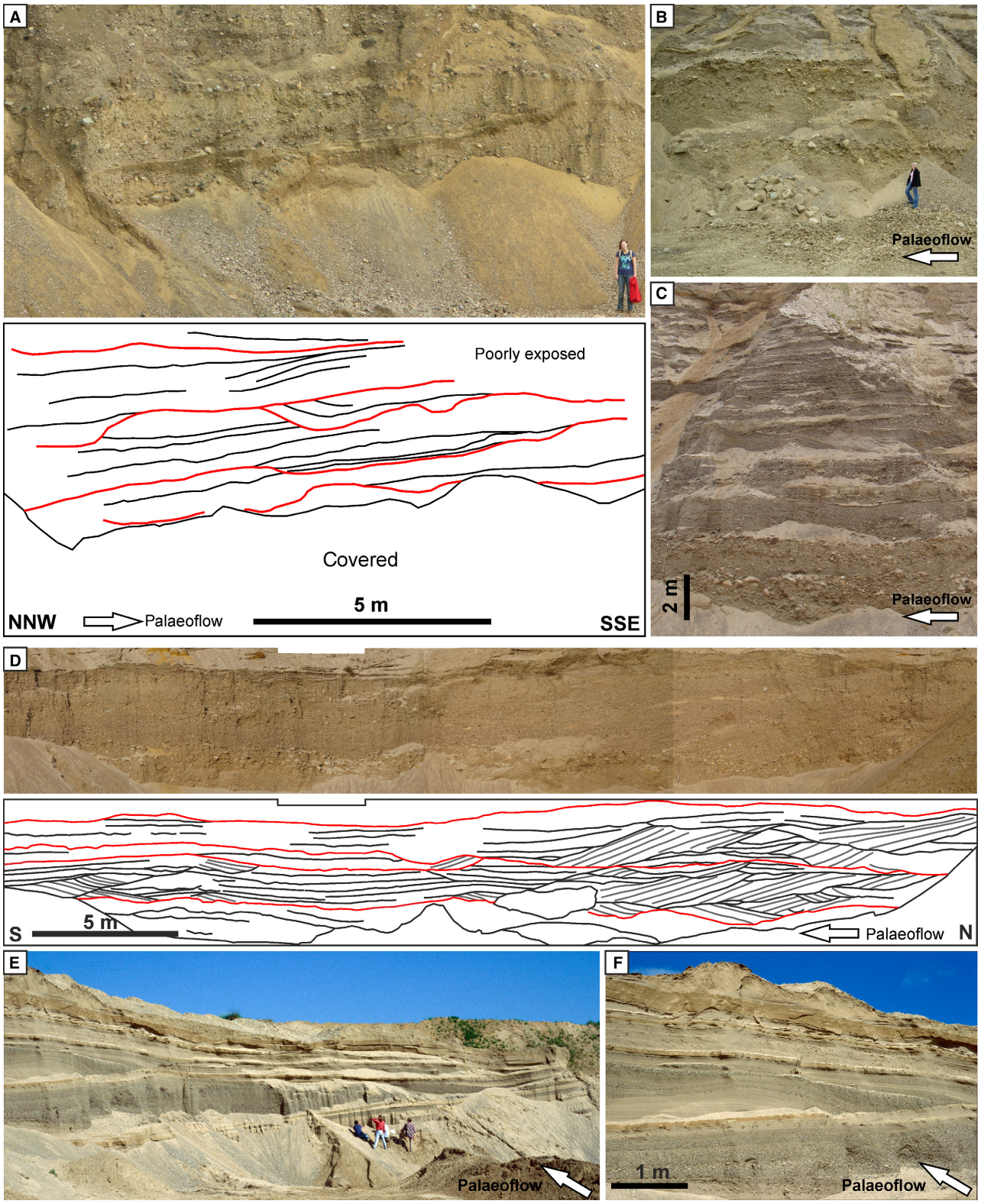

comprising antidune and chute-and-pool deposits (Fig. 6). Antidune deposits are characterized by tabular or lenticular concave-up bedsets that are conformably overlying concave-up basal surfaces. Based on outcrop observations, Duller *et al.* (2008) reconstructed antidune wavelengths

Fig. 7. Upper-flow-regime bedforms in gravel-rich subaqueous ice-contact fan deposits (A) to (D) Porta Fan, northern Germany; Middle Pleistocene; (E) and (F) Coppenbrügge Fan, northern Germany; Middle Pleistocene). (A) Interpreted 'photo panel' from proximal gravel-rich fan deposits. Highly scoured amalgamated gravel of the proximal fan mouth bar are interpreted as deposited by expanding supercritical flows. The upflow dip of the higher-order erosional surfaces (red) may indicate deposition on the ice-proximal side of the mouth bar. (B) Close-up of the scoured gravel in the proximal gravel-rich fan deposits. Person for scale is *ca* 1.6 m. (C) Scoured pebble to cobble gravel, passing upward into backset and foreset cross-stratified and subhorizontally stratified pebble gravel, indicating deposition by chutes-and-pools or breaking antidunes. (D) Interpreted 'photo panel' from distal gravel-rich fan deposits. The succession comprises lenticular scours with gravelly backsets or foresets, indicating deposition by hydraulic jumps and sheet-like low-angle cross-stratified gravel, interpreted as breaking antidune deposits (modified from Lang *et al.*, 2017b). (E) Thinning-upward and fining-upward succession of sinusoidally stratified gravelly to sandy stable antidune deposits. (F) Detail of the antidune deposits. Note the spaced stratification style and convex-up geometry of the bedforms.

ranging from 24 to 96 m and amplitudes of up to 1.3 m. Deposits of chutes-and-pools form convex-up bedsets that infill deep, steep-walled scours up to 13 m long and 3 m deep (Fig. 6A and B) Antidunes are interpreted to have been the dominant bed configurations during the waxing and waning stages of the jökulhlaup, while chutes-and-pools formed during peak flood conditions (Duller *et al.*, 2008). Similar jökulhlaup deposits were described by Girard *et al.* (2015) from an Upper Ordovician glacifluvial delta-plain succession in Libya. Antidune deposits comprise up to 20 m thick, sinusoidally and subhorizontally stratified pebbly sandstone, displaying wavelengths of up to 100 m and amplitudes of up to 5 m (Girard *et al.*, 2015). The distal equivalents of these deposits are deposits of antidunes and climbing dunes in sandstones accumulated at the delta front and hybrid-event beds on the delta slope (Girard *et al.*, 2012a, 2012b).

Scour fills related to isolated hydraulic jumps were described from Icelandic jökulhlaup deposits by Burke *et al.* (2010a). Scours are 40 to 70 m long, 15 to 20 m wide and 3 to 7 m deep. Internally, the scour fills comprise cobble to boulder gravel, forming foresets on the lee sides and backsets on the stoss sides. Hydraulic jumps are interpreted to have formed upstream of stranded ice blocks that acted as flow obstacles, leading to scouring and deposition around the ice blocks (Burke *et al.*, 2010a).

Subaqueous depositional environments

Bedforms related to supercritical density flows are common in deposits of glacilacustrine or glacimarine subaqueous ice-contact fans, deltas and glacigenic deep-water fans (Fig. 1B; Table 1). A major distinction between glacilacustrine and glacimarine settings is given by the density difference between freshwater and seawater, affecting the density contrast between a sediment-laden flow and the ambient water and hence the mechanics of sediment transport by density flows. Glacilacustrine settings may be more favourable to generate hyperpycnal flows due to the relatively low density of their ambient water (Russell & Arnott, 2003; Winsemann *et al.*, 2009; Lang *et al.*, 2017b), while glacimarine settings may foster the formation of buoyant plumes (Powell, 1990; Dowdeswell *et al.*, 2015).

Subaqueous ice-contact fans

Subaqueous ice-contact fans (also known as grounding-line fans) are fed by meltwater discharging from englacial or subglacial conduits of grounded ice margins into glacilacustrine or glacimarine basins (Fig. 1B) (Rust & Romanelli, 1975; Powell, 1990; Gorrell & Shaw, 1991; Lønne, 1995; Le Heron *et al.*, 2004; Hornung *et al.*, 2007; Winsemann *et al.*, 2009; Deschamps *et al.*, 2013; Aquino *et al.*, 2016). The meltwater effluent behaves as a jet when entering a standing water body (Powell, 1990). Jets are momentum-driven flows that evolve into gravity-driven flows due to the turbulent entrainment of ambient water, leading to flow expansion and deceleration (Bates, 1953; Launder & Rodi, 1983; Hoyal *et al.*, 2003). Glacigenic jets with very high discharge and momentum may relate to outbursts of large volumes of meltwater from subglacial or englacial reservoirs (Russell & Arnott, 2003; Hornung *et al.*, 2007; Winsemann *et al.*, 2009; Dowdeswell *et al.*, 2015).

The meltwater jet erodes large-scale scours that laterally transition into proximal fan-deposits. The geometries of the scour and of the fan are controlled by the densimetric Froude number at the outlet, by sediment-grain size and aggradation rate (Lang *et al.,* in review; Powell, 1990; Hoyal *et al.*, 2003). Winsemann *et al.*

(2009) documented large-scale (1.3 to 3.2 km long, 0.8 to 1.2 km wide, 7 to 25 m deep) scours that radiate from the former meltwater outlet and pass downflow into proximal gravel-rich fan lobes of a Pleistocene glacilacustrine ice-contact fan. The scours closely resemble those formed by experimental jets (Lang *et al.,* in review; Hoyal *et al.*, 2003) and are interpreted to indicate outlet densimetric Froude numbers larger than five (Winsemann *et al.*, 2009). Proximal gravel-rich fan lobes are interpreted as the mouth bars of the glacigenic jet flow and are unconformably overlain by more distal sand-rich lobes deposited by sustained density flows on the lee side of and between the gravelly mouth bars (Hornung *et al.*, 2007; Winsemann *et al.*, 2009; Lang & Winsemann, 2013; Lang *et al.*, 2017b). Deposits of supercritical flow are very common within gravelly and sandy subaqueous ice-contact fan deposits and may be considered characteristic facies for these systems (Figs 3, 7 and 8) (Brennand, 1994; Russell *et al.*, 2003; Hornung *et al.*, 2007; Russell *et al.*, 2007; Winsemann *et al.*, 2009; Lang & Winsemann, 2013; Leszczynska *et al.*, 2017, 2018; Lang *et al.*, 2017b).

The large-scale geometry of gravel-rich fan deposits is wedge-shaped, with an overall gentle (3 to 5°) glacierward dip on the proximal side and basinward dip on the distal side (Lønne, 1995, 2001; Hornung *et al.*, 2007; Russell *et al.*, 2007; Winsemann *et al.*, 2009). The most proximal fan deposits are characterized by highly scoured gravel (Fig. 7A to C). The largest and most proximal scour fills commonly display both foreset and backset cross-stratification, interpreted as the progradational infill of the scours or as deposits of local hydraulic jumps (Winsemann *et al.*, 2009; Lang *et al.*, 2017b). Scours are probably formed during an early flow-stage and relate either to the impingement of eddies generated by the expanding meltwater jet or slope failures on the inner margin of the mouth bar (Lang *et al.,* in review; Lang *et al.*, 2017b). Distally, scours become smaller and are associated with more sheet-like deposits, forming vertical and lateral stacks characterized by erosional contacts. Scour fills comprise backset or foreset cross-stratification or concentric concave-up stratification, indicating deposition by chutes-and-pools, isolated hydraulic jumps or breaking antidunes (Fig. 7C and D) (Lang *et al.*, 2017b). Sheet-like deposits consist of low-angle cross-stratified, subhorizontally or sinusoidally stratified gravel formed by breaking or non-breaking antidunes (Brennand, 1994; Russell & Arnott, 2003; Leszczynska *et al.*, 2017, 2018; Lang *et al.*, 2017b). Planar and trough cross-stratified gravel indicates the migration of 2D and 3D gravel dunes under high-energy subcritical flows (Russell & Arnott, 2003; Hornung *et al.*, 2007; Winsemann *et al.*, 2009; Lang *et al.*, 2017b).

Sand-rich fan deposits form gently (<15°) downflow dipping beds (Fig. 3) (Gorrell & Shaw, 1991; Hornung *et al.*, 2007; Winsemann *et al.*, 2007a, 2009; Lang *et al.*, 2017b; Virtasalo *et al.*, 2019). Slopes of subaqueous ice-contact fans may become steeper in basins with high topographic gradients (Lønne, 1995) or where subaqueous ice-contact fans prograde in confined settings (Deschamps *et al.*, 2013). Internally, the sand-rich fan deposits may comprise laterally and vertically stacked lobe elements with a recurring internal architecture probably controlled by autogenic flow morphodynamics (Lang *et al.*, 2017b). Low-angle cross-stratified, subhorizontally or sinusoidally stratified sand and pebbly sand, pointing to deposition by aggrading quasi-stationary antidunes, represent the typical facies association of these sand-rich fan deposits (Figs 3 and 8). These antidune deposits are associated with facies representative of chutes-and-pools and humpback dunes. Chute-and-pool deposits are characterized by scours filled by diffusely stratified or backset cross-stratified pebbly sand and occur both as isolated and as amalgamated stacks. They are commonly associated with laterally extensive erosional surfaces (Fig. 8A and B) (Gorrell & Shaw, 1991; Russell & Arnott, 2003; Russell *et al.*, 2007; Winsemann *et al.*, 2009; Lang & Winsemann, 2013; Leszczynska *et al.*, 2017; Lang *et al.*, 2017b). Lateral and vertical transitions from sigmoidally cross-stratified humpback dunes into sinusoidally stratified antidune deposits are common (Fig. 8D) (Russell *et al.*, 2007; Lang & Winsemann, 2013; Lang *et al.*, 2017b). Distally, thick successions of trough cross-stratified pebbly sand and climbing-ripple cross-laminated sand indicate deposition of dunes and climbing ripples by subcritical flows under high rates of suspension fall-out (Powell, 1990; Russell & Arnott, 2003; Winsemann *et al.*, 2009; Deschamps *et al.*, 2013).

Glacigenic deltas

Glacigenic deltas are formed by meltwater discharge at the shorelines of glacilacustrine or glacimarine basins (Fig. 1A). Glacigenic deltas may be classified based on their position relative to the ice margin and by the gradient and

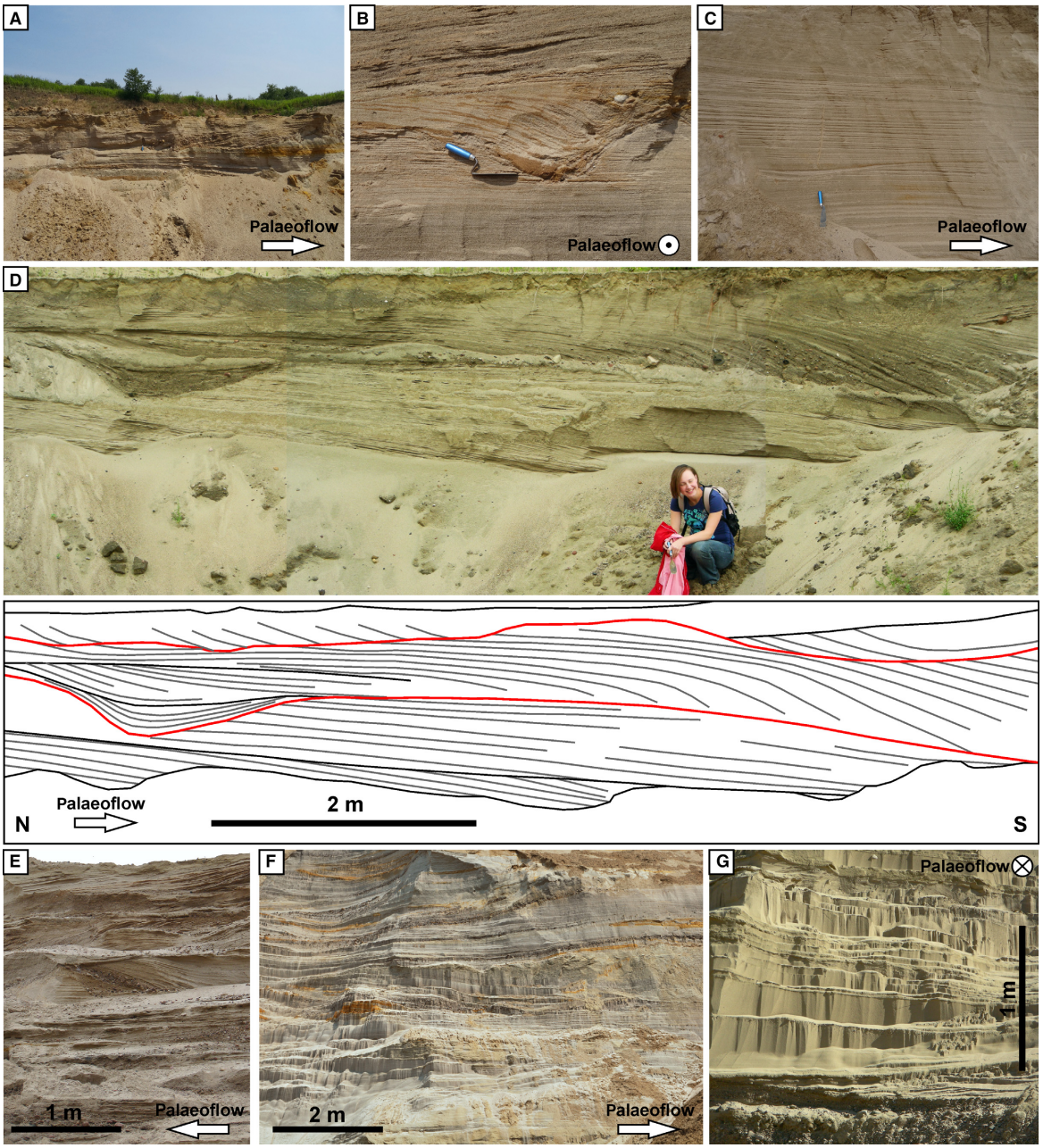

Fig. 8. Sand-rich subaqueous ice-contact fan deposits (Porta Fan, Middle Pleistocene; northern Germany). (A) Sinusoidally stratified antidune deposits separated by an irregular scour surface. Pebbles and sandy intraclasts occur at the scour surface. Trowel for scale is 28 cm. (B) Concentric scour fill, pointing to an isolated hydraulic jump (chute-and-pool deposit) at the contact between sinusoidally stratified antidune deposits. Trowel for scale is 28 cm. (C) Antidune deposits, comprising sinusoidally stratified fine-grained to medium-grained sand. Note internal erosive truncation (above trowel) and pinch-and swell of laminae. Trowel for scale is 28 cm. (D) Interbedded deposits of chutes-and-pools, antidunes and humpback dunes. Sinusoidally stratified antidune deposits form the lower part of the succession. The concentric scour fill in the left centre indicates an isolated hydraulic jump (chute-and-pool). Sigmoidal cross-stratification (upper right) points to deposition by humpback dunes. (E) Interbedded deposits of chutes-and-pools and antidunes. Note the steep-walled scour filled by three generations of backsets in the centre. Lateral (upflow) fining of backsets points to upflow migration of the hydraulic jump during chute-and-pool formation. (F) Sinusoidally stratified and low-angle cross-stratified sandy antidune deposits, forming packages that are 0.5 to 1.5 m thick and fine upward. Contacts between packages are erosional and commonly overlain by gravel. (G) Structureless inversely graded beds, forming part of antidune deposits. This stratification style indicates deposition from high-density flows.

accommodation space at the receiving basin margin. Ice-contact deltas are deposited directly at the ice margin and are characterized by a short and poorly developed subaerial delta plain, while glacifluvial deltas have well-developed delta plains and may develop at a considerable distance from the ice margin (Lønne, 1995). Ice-contact deltas are commonly characterized by coarse-grained gravity-flow deposits, including flow tills and resedimented till clasts. During progradation, ice-contact deltas may evolve into glacifluvial deltas (Lønne, 1995). High-gradient settings allow for the deposition of Gilbert-type deltas, displaying longitudinal profiles with a distinctive subdivision into topset, foreset and bottomset deposits, while low-gradient settings feature shoal-water deltas dominated by subaqueous mouth-bar complexes (Ashley, 1995; Winsemann *et al.*, 2018). Depositional processes in deltas include tractional flows, sustained and surge-type, high-density and low-density turbidity currents, cohesionless debris flows and suspension fall-out (Nemec, 1990; Mulder & Alexander, 2001; Winsemann *et al.*, 2011, 2018; Gobo *et al.*, 2014, 2015).

Upper-flow-regime bedforms commonly occur within deposits of glacifluvial deltas (Fig. 3; Table 1) (Postma *et al.*, 1983; Winsemann *et al.*, 2011, 2018; Girard *et al.*, 2012a,b; Dietrich *et al.*, 2016, 2017; Moreau & Joubert, 2016; Nehyba *et al.*, 2017; Normandeau *et al.*, 2017; Lang *et al.*, 2017b; Hanáček *et al.*, 2018; Leszczynska *et al.*, 2018; Kostic *et al.*, 2019). The successions are very similar to those described from non-glacigenic coarse-grained deltas (e.g. Nemec, 1990; Gobo *et al.*, 2014, 2015; Ventra *et al.*, 2015; Massari, 2017; Kostic *et al.*, 2019; Okazaki *et al.*, 2020; Postma *et al.*, 2020). The formation of upper-flow-regime bedforms is favoured by steep delta slopes of 5 to 35° (Lønne, 1995; Dietrich *et al.*, 2017; Winsemann *et al.*, 2018), by far exceeding the necessary threshold of 0.45 to 0.6° for submerged density flows to attain supercritical conditions (Sequeiros, 2012; Covault *et al.*, 2017). Further parameters leading to the formation of upper-flow-regime bedforms are: (i) the occurrence of high-magnitude outburst floods (Girard *et al.*, 2012a,b); (ii) rapid high-magnitude lake-level falls, triggering incision and bypass of coarse-grained sediment to the delta toe that commonly involve supercritical flows (Winsemann *et al.*, 2011, 2016, 2018); and (iii) flow strength amplified by tidal drawdown (Dietrich *et al.*, 2017).

Glacifluvial distributary systems on delta plains may display upper-flow-regime bedforms similar to those described in other glacifluvial systems (Fig. 3). Girard *et al.* (2012a,b) documented subaerial and subaqueous delta-plain deposits that comprise up to 10 m thick packages of sinusoidally and (sub-)horizontally stratified sandstones, partly forming undulating bedforms with wavelengths of up to 40 m, interpreted as the product of antidunes formed during the early waning stages of jökulhlaups. Antidune deposits are commonly associated with metre-scale scours filled by intraformational conglomerates that point to bypass and cut-and-fill processes (Girard *et al.*, 2012a,b), probably related to chutes-and-pools. Dietrich *et al.* (2017) described antidune deposits from the infill of braided channels in Pleistocene subtidal delta-plain deposits in Canada. Antidune deposits comprise subhorizontally stratified pebbly sand, forming undulating bedforms with wavelengths between 5 m and 10 m (Dietrich *et al.*, 2017).

Base-level fall may lead to the dissection of delta plains and slopes and to the formation of incised valleys (Fig. 9A). In glacilacustrine settings, very rapid high-magnitude lake-level falls may occur due to the opening of outlet channels (Winsemann *et al.*, 2011, 2018). The initial valley incision may relate to the formation of (net-erosional) cyclic steps (Strong & Paola, 2008; Winsemann *et al.*, 2011, 2018; Muto *et al.*, 2012; Kostic *et al.*, 2019). Examples of such incised valleys related to lake-level falls include symmetrical to slightly asymmetrical bedforms (wavelength of *ca* 60 to 90 m) associated with isolated scour fills and interpreted as representing cyclic steps or antidunes (Winsemann *et al.*, 2011, 2018; Kostic *et al.*, 2019). Scours infilled by gravelly backsets occur along erosional surfaces related to forced regression and point to deposition in the hydraulic-jump zone of cyclic steps (Fig. 9A) (Kostic *et al.*, 2019).

Upper-flow-regime bedforms on delta slopes are deposited by both surge-type and sustained turbidity currents. Deposits of surge-type supercritical turbidity currents are characterized by backset cross-stratified gravelly or sandy scour fills, interpreted as deposits of the hydraulic-jump zone of cyclic steps, associated with low-angle cross-stratification or sinusoidal stratification in pebbly sand or sand, pointing to deposition by antidunes (Fig. 9B) (Lang *et al.*, 2017b; Winsemann *et al.*, 2018; Kostic *et al.*, 2019). Scour fills related to hydraulic jumps are commonly widely spaced and isolated, indicating deposition at the lower limit of the cyclic-step

stability field or to aggradation associated with the local development of chutes-and-pools (Fig. 10) (Massari, 2017; Lang *et al.*, 2017a,b). Cyclic-step and antidune deposits commonly form the basal part of fining-upward successions and are overlain by ripple cross-laminated sand (Lang *et al.*, 2017b; Winsemann *et al.*, 2018), pointing to deposition by waning flows (Mulder & Alexander, 2001). Surge-type turbidity currents are probably triggered by frequent small-volume slope failures along the upper delta slope (Hughes Clarke, 2016), favoured by high aggradation rates (Gobo *et al.*, 2014, 2015; Winsemann *et al.*, 2018).

Deposits of sustained supercritical density flows are characterized by laterally extensive trains of scours filled by backset cross-stratified pebbly sand, probably deposited by cyclic steps

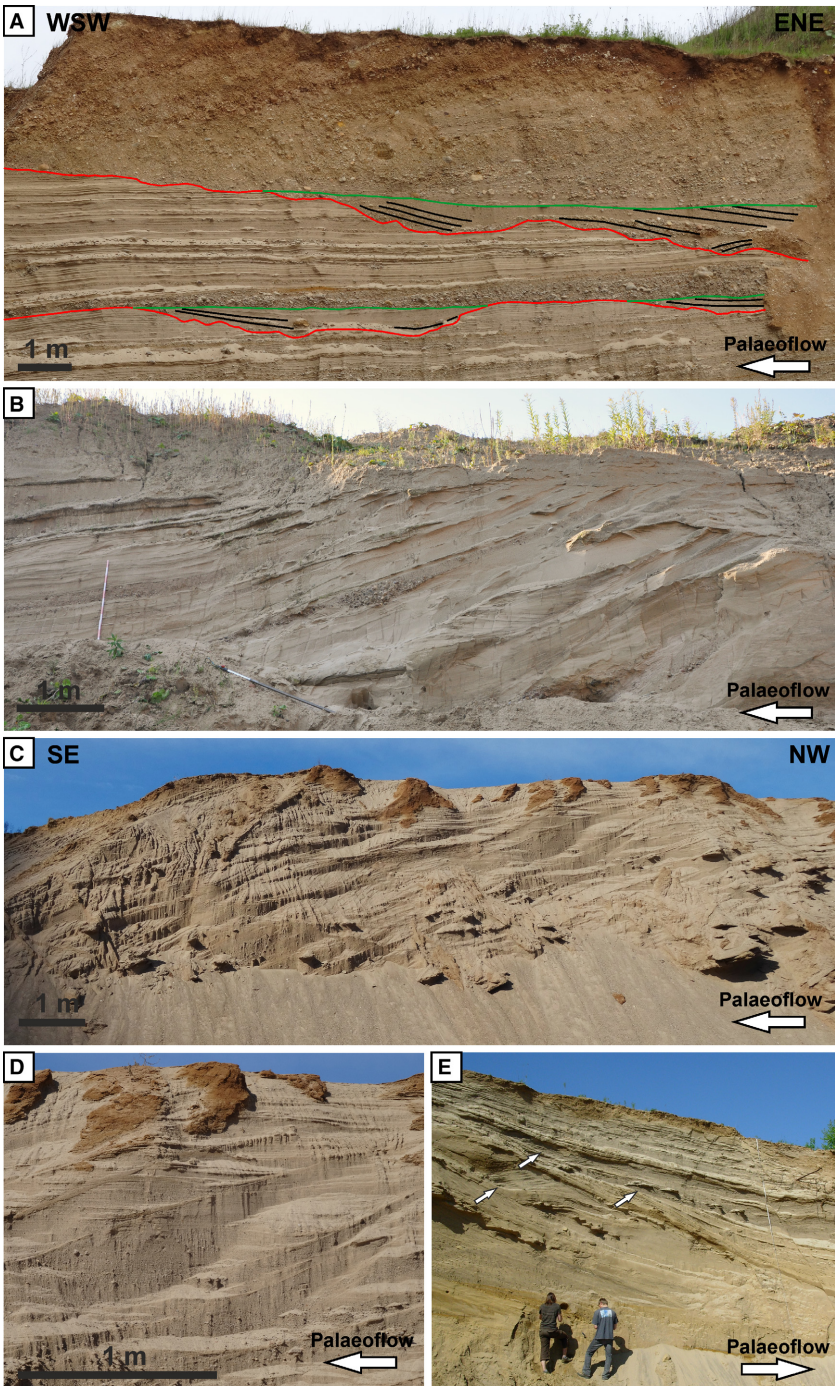

Fig. 9. Upper-flow-regime bedforms in glacifluvial deltas. (A) Deposits of cyclic steps overlie erosional surfaces (red) formed during forced regression. Cyclic-step deposits comprise elongate scours filled by backsets. Prograding delta-foreset deposits downlap the erosional surfaces and cyclic-step deposits (Betheln Delta, northern Germany; Middle Pleistocene; modified from Kostic *et al.*, 2019). (B) Delta-foreset deposits, comprising, isolated gravelly and sandy backset cross-stratified scour fills, which are interbedded with sinusoidally stratified sand. The succession is interpreted as deposits of cyclic steps and superimposed antidunes that were formed by surge-type supercritical density flows. Tool for scale is 1.4 m (Porta Delta, northern Germany; Middle Pleistocene). (C) Delta-foreset deposits, comprising laterally stacked scours filled by backset cross-stratified pebbly sand interpreted as cyclic steps deposited by sustained supercritical density flows (Freden Delta; northern Germany; Middle Pleistocene). (D) Detail of the stacked backset cross-stratified scour fills from Fig. 5C. (E) Isolated backset cross-stratified scour-fills (arrows) related to cyclic steps within foreset packages dominated by climbing-ripple cross-laminated sand (Freden Delta, photograph by courtesy of C. Brandes; modified from Lang *et al.*, 2017b, and Winsemann *et al.*, 2018).

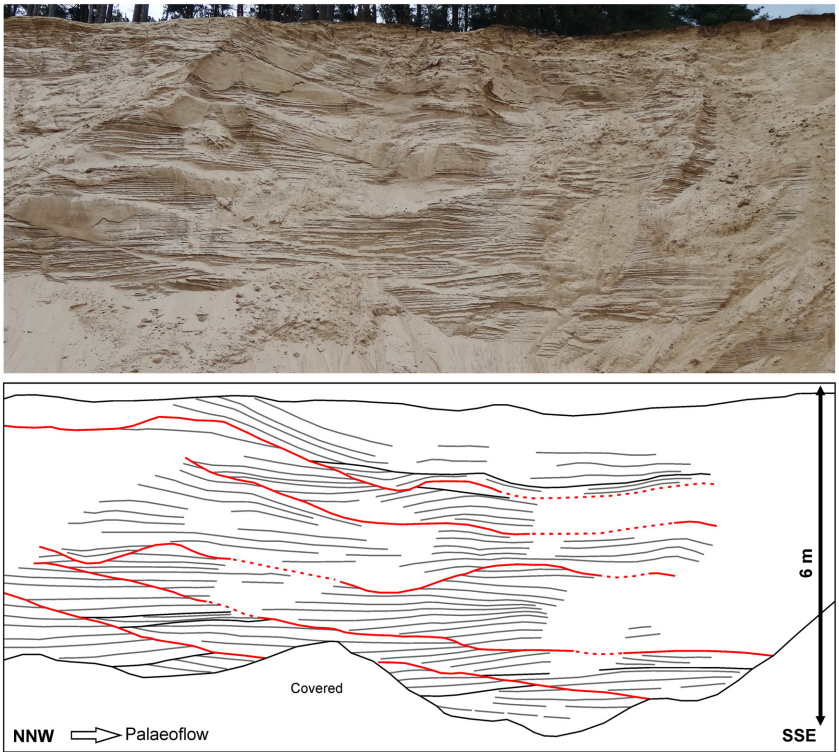

Fig. 10. Sand-rich glacifluvial delta sediments deposited by chutes-and-pools and antidunes (Westeroden Delta, northern Germany; Middle Pleistocene). Scour fills above higher-order bounding surfaces (red) indicate isolated hydraulic-jump zones. Low-angle cross-stratification and sinusoidal stratification characterize antidune deposits. Lower-order bounding surfaces (black) indicate truncations within antidune packages.

(Fig. 9C to E) (Dietrich *et al.*, 2016; Lang *et al.*, 2017b; Winsemann *et al.*, 2018; Kostic *et al.*, 2019). The scours may amalgamate to form laterally extensive downflow-dipping composite erosion surfaces ('pseudo-foresets', Dietrich *et al.*, 2016). Backsets in cyclic-step deposits may pass downflow into low-angle cross-stratified or sinusoidally stratified pebbly sand or sand deposited by antidunes (Fig. 9C) (Dietrich *et al.*, 2016, 2017; Lang *et al.*, 2017b; Winsemann *et al.*, 2018). Some foreset beds consist entirely of antidune deposits (Fig. 10). Cyclic-step and antidune deposits are associated with sandy foreset beds, comprising deposits of humpback dunes, (climbing) dunes and climbing ripples (Dietrich *et al.*, 2016; Lang *et al.*, 2017b; Winsemann *et al.*, 2018). Sustained density flows on steep subaqueous slopes can stay supercritical and form hydraulic jumps at the base of the slopes (Komar, 1971; Clemmensen & Houmark-Nielsen, 1981; Mutti & Normark, 1987; Nielsen *et al.*, 1988; Dabrio *et al.*, 1991; Winsemann *et al.*, 2007b; Covault *et al.*, 2017; Rubi *et al.*, 2018). Hydraulic jumps may also form on the slopes of Gilbert-type deltas, resulting in the formation of local scours filled with backsets or massive deposits, surrounded by or passing upslope into diffusely stratified, low-angle stratified or spaced planar stratified sand or pebbly sand in the upper or middle part of the foreset bed (Clemmensen & Houmark-Nielsen, 1981; Nemec, 1990; Massari, 1996, 2017; Dietrich *et al.*, 2016; Selim, 2019; Okazaki *et al.*, 2020). Hydraulic jumps formed on the upper part of the slope may also trigger the formation of upslope-migrating climbing-ripples on the lower delta slope due to large backflow areas (Clemmensen & Houmark-Nielsen, 1981; Winsemann *et al.*, 2007b, 2018). The slope of these Gilbert-type deltas commonly varies between 5° and 26° and is thus well below the angle of repose, excluding grain-flow avalanches as a cause of the diffuse stratification or spaced planar stratification. Therefore, diffuse stratification and spaced planar stratification are interpreted to represent conditions of high densimetric Froude numbers in sustained density flows (Fedele *et al.*, 2016).

Sustained supercritical density flows are triggered by sediment-laden flows, plunging over the delta brink and evolving into hyperpycnal flows. The formation of hyperpycnal flows is commonly interpreted as related to high-discharge events (Ventra *et al.*, 2015; Carvalho & Vesely, 2017), such as jökulhlaups (Ghienne *et al.*, 2010; Girard *et al.*, 2012a,b). Deposits pointing to sustained density flows are favoured in settings where the delta plain is bypassed during lake-level lowstand or highstand when

accommodation is low (Lang *et al.*, 2017b; Winsemann *et al.*, 2018).

Downslope, the steeply dipping foreset beds typically pass into gently dipping to flat toeset and bottomset beds. The slope break at the transition may trigger hydraulic jumps in supercritical density flows, leading to the formation of isolated scours filled by backsets or massive deposits, which may be incised into finer-grained delta-foreset or toeset deposits (Fig. 7E) (Winsemann *et al.*, 2007b, 2018; Leszczynska *et al.*, 2018). Increased sedimentation rates downflow of hydraulic jumps may cause the accumulation of thick successions featuring climbing-dune cross-stratification and climbing-ripple cross-lamination in the delta toeset (Winsemann *et al.*, 2011, 2018).

Glacigenic subaqueous fans

Glacigenic subaqueous fans are deposited by glacigenic density flows and are common in deep-water glacimarine successions, where they extend downdip from subaqueous ice-contact fans or deltas (Fig. 3; Table 1) (Lønne, 1997; Plink-Björklund & Ronnert, 1999; Lajeunesse & Allard, 2002; Le Heron *et al.*, 2010; Hirst, 2012; Lang *et al.*, 2012; Dietrich *et al.*, 2017, 2019; Normandeau *et al.*, 2017).

Successions comprise sheet-like sediment bodies that represent depositional lobes (Lønne, 1997; Plink-Björklund & Ronnert, 1999; Le Heron *et al.*, 2004, 2006; Hirst, 2012; Dietrich *et al.*, 2017) or ribbon-shaped sediment bodies that represent the infills of channels (Hirst *et al.*, 2002; Hirst, 2012; Girard *et al.*, 2012a,b). The most commonly reported upper-flow-regime bedforms from deposits of glacimarine subaqueous fans are antidunes (Fig. 11) (Hirst *et al.*, 2002; Le Heron *et al.*, 2010; Hirst, 2012; Lang *et al.*, 2012; Girard *et al.*, 2012a,b). The sedimentary facies of glacimarine lobe deposits are very similar to those of non-glacigenic unconfined supercritical density flows, whose facies signatures are typically dominated by antidune deposits (Lang *et al.*, 2017a; Postma & Kleverlaan, 2018; West *et al.*, 2019). Antidune deposits comprise sinusoidally stratified fine-grained sandstone with wavelengths from 1.5 to 3.5 m and amplitudes from 0.1 to 0.25 m, forming up to 5 m thick vertical stacks with antidune crests displaying upflow or downflow migration (Fig. 11A to C) (Hirst *et al.*, 2002; Hirst, 2012). Antidune deposits are associated with deposits of chutes-and-pools and humpback dunes. Deposits of chutes-and-pools are characterized by steep-walled scours filled by partly deformed backsets (Fig. 11B). Humpback dunes display sigmoidal cross-stratification and may be laterally and/or vertically transitional to sinusoidally stratified antidune deposits (Fig. 11D) (Hirst, 2012; Le Heron *et al.*, 2013).

DISCUSSION

Characteristic dimensions of bedforms and sedimentary structures

The compilation of the documented field examples (Table 1) provides an overview of the occurrence of upper-flow-regime deposits in different glacigenic depositional environments and of their characteristic dimensions. The formation and preservation of the different bedform types relate to environment-controlled parameters like flow depth, flow velocity and aggradation rate, and to their temporal and spatial evolution. Upper-stage-plane beds are documented from glacifluvial systems, where aggradation rates are comparatively low and bedforms are thus poorly preserved. Deposits of antidunes are documented from all studied glacigenic depositional environments, although their architecture and dimensions are highly variable, depending on the respective setting. Cyclic-step deposits occur in successions from deltas and glacial lake-outburst floods. Chute-and-pool deposits were observed in successions from glacifluvial systems, subaqueous (ice-contact) fans and glacial lake-outburst floods. However, the distinction between deposits of cyclic steps and chutes-and-pools may be ambiguous (cf. Lang & Winsemann, 2013; Postma *et al.*, 2020). Some sedimentary structures interpreted as cyclic-step deposits (Fig. 9B) may also represent deposits of chutes-and-pools, and vice versa (Fig. 10) (Massari, 2017; Lang *et al.*, 2017a; Okazaki *et al.*, 2020).

Dimensions that are commonly considered characteristic for different bedforms and sedimentary structures can also be linked to flow parameters, including the wavelength and wave steepness of bedforms, and aspect ratio and spacing of scours (Kennedy, 1963; Hand, 1974; Cartigny *et al.*, 2014; Fedele *et al.*, 2016). Wavelength and wave steepness can only be measured from well-preserved deposits, while values of aspect ratio and spacing of scours can also be obtained from less complete successions (Symons *et al.*, 2016). In glacigenic depositional

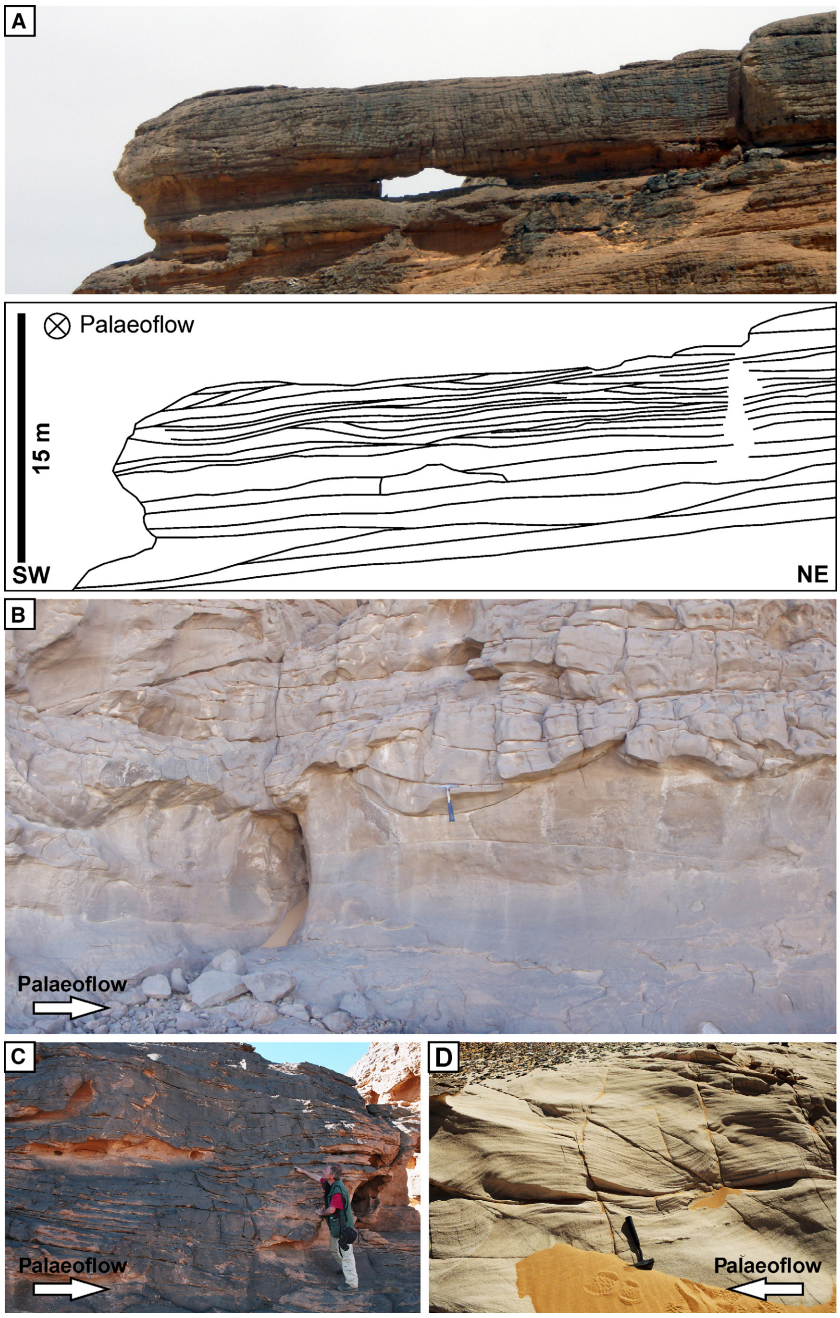

Fig. 11. Upper-flow-regime bedforms deposited by supercritical density flows in glacimarine settings (North Africa; Upper Ordovician). (A) Sheet-like sandstones that display sinusoidal stratification and low-angle cross-stratification with common internal low-angle truncations, pointing to deposition by antidunes (Jebel Asba region, Kufra Basin, Libya). (B) Thickly bedded sinusoidally stratified sandstone, indicating highly aggrading antidune deposits, is unconformably overlain by foreset and backset cross-stratified sandstone, probably indicating chutes-and-pools. Hammer for scale is 33 cm (Jebel Eghei region, Kufra Basin, Libya; from Le Heron *et al.*, 2014). (C) Sinusoidally stratified sandstone deposited by antidunes (Tassili N'Ajjer region, Illizi Basin, Algeria). (D) Sigmoidally stratified sandstone deposited by humpback dunes, passing upward into sinusoidally stratified antidune deposits. Hammer for scale is 33 cm (Jebel Asba region, Kufra Basin, Libya; from Le Heron *et al.*, 2010).

environments, bedform wavelength and steepness are documented from deposits of cyclic steps, chutes-and-pools and non-breaking antidunes (Table 1). Cyclic-step wavelengths from the slopes of glacigenic deltas vary over three orders of magnitude (Fig. 12A). Shorter wavelengths relate to coarse-grained systems with steep gradients, while longer wavelengths relate to fine-grained systems with gentle gradients. The linkage between grain size and slope and bedform wavelength is in line with other studies of experimental and natural bedforms (Kostic, 2011; Slootman & Cartigny, 2019). If deposits of cyclic steps and antidunes occur in the same depositional system, cyclic-step wavelengths are one order of magnitude larger than antidune wavelengths (Fig. 12A), matching the results of numerical simulations by Kostic (2014) and Kostic *et al.* (2019).

The wavelength of antidunes and their deposits scales with the flow depth (Kennedy, 1963; Hand, 1974). The variation of antidune

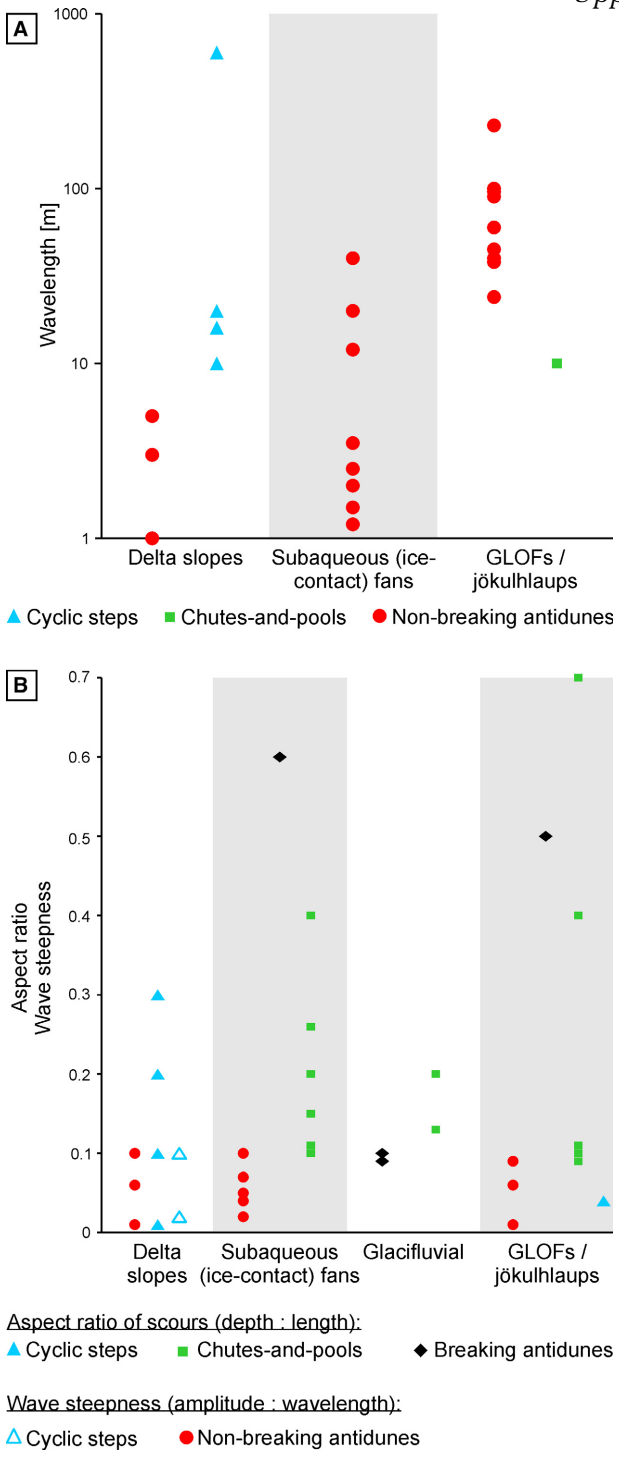

Fig. 12. Upper-flow-regime bedform dimensions measured in different glacigenic depositional environments. (A) Wavelengths of different bedform types. (B) Aspect ratios and wave steepness of different bedform types (GLOF, glacial lake-outburst flood).

wavelengths over three orders of magnitude (Fig. 12A) can thus be explained by strong variations of the flow velocities and depths between different environments. Glacigenic deltas are rather small systems, but their steep slopes will cause strong acceleration of flows (e.g. Dietrich *et al.*, 2016; Lang *et al.*, 2017b; Winsemann *et al.*, 2018). Relatively shallow fast flows will cause high densimetric Froude numbers that may trigger antidune-wave breaking (Kennedy, 1963), potentially resulting in a transition to cyclic steps (Fedele *et al.*, 2016). Jökulhlaups or glacial lake-outburst floods are characterized by high-magnitude, deeper flows (Duller *et al.*, 2008; Alho *et al.*, 2010; Winsemann *et al.*, 2011, 2016; Girard *et al.*, 2012a,b; Lang *et al.*, 2019), leading to the formation of correspondingly long wavelength bedforms (Fig. 12A). Antidune deposits in subaqueous (ice-contact) fans display a wide range of wavelengths (Fig. 12A), indicating that a wide range of flow magnitudes may occur in these depositional systems. Previous field-based studies suggested that longer wavelength bedforms relate to higher-magnitude events (Hirst *et al.*, 2002; Russell & Arnott, 2003; Lang & Winsemann, 2013; Lang *et al.*, 2017b).

The wave steepness (wave height/wavelength) of antidune and cyclic-step deposits is fairly similar in all studied depositional environments (Fig. 12B). Antidune deposits have wave steepness values consistently lower than 0.1, which is below the experimentally determined critical antidune-wave steepness of 0.142 (Kennedy, 1963). If antidune-wave steepness exceeds the critical value, wave breaking and reworking of the bed will occur (Kennedy, 1963; Middleton, 1965). Therefore, it is not surprising that the steepness of preserved bedforms is well below the critical value.

The aspect ratios (depth/length) of scours related to cyclic steps, chutes-and-pools and breaking antidunes show no clear trends or relation to the depositional environments (Fig. 12B). Scours interpreted as formed by cyclic steps tend to display lower and less variable aspect ratios, while other bedform types display a wider range of values.

Controls on the formation and preservation of upper-flow-regime bedforms

The documented bedforms and bedform successions from glacigenic settings are very similar to those known from non-glacigenic settings. The great diversity of glacigenic depositional environments allows for the study of bedforms and sedimentary facies deposited under a wide range of flow conditions and sediment supply. The

differences in the observed sedimentary facies are controlled by various parameters, including: (i) slope; (ii) confined versus unconfined conditions; (iii) sediment concentration and aggradation rate; (iv) dominant grain size; and (v) discharge variations. However, all of these controlling factors relate to parameters that characterize the respective depositional system but are not specific for glacigenic settings. Observations from glacigenic depositional environments can therefore be transferred to non-glacigenic depositional environments, and vice versa. Glacifluvial systems can be compared to other high-energy ephemeral alluvial or fluvial systems (Blair, 1999; Fielding, 2006; Froude *et al.*, 2017; Carling & Leclair, 2019; Wang & Plink-Björklund, 2020). Glacigenic Gilbert-type deltas display the same facies types and depositional architectures as non-glacigenic Gilbert-type or fan deltas (Massari, 2017; Kostic *et al.*, 2019; Okazaki *et al.*, 2020; Postma *et al.*, 2020), as do glacigenic density flows and non-glacigenic density flows (Lang *et al.*, 2017a; Ono & Plink-Björklund, 2018; West *et al.*, 2019). Proximal subaqueous ice-contact fans and ice-contact deltas may represent an exception here, because they only occur in glacigenic settings and their deposition is controlled by specific ice-marginal conditions. However, the medial to distal reaches of glacigenic subaqueous ice-contact fans are characterized by density flows that present the same dynamics as in non-glacial settings (Lang *et al.*, 2012, in review; Powell, 1990; Hirst, 2012). Glacial lake-outburst-floods may affect all glacigenic depositional environments, commonly leading to very high-magnitude flows and to the formation of exceptionally large bedforms (Duller *et al.*, 2008; Winsemann *et al.*, 2011, 2018; Girard *et al.*, 2012a,b; Carling, 2013).

Bed slope and flow confinement

The bed slope controls flow acceleration by gravity, and thus has a huge impact on bedform evolution. Steep gradients, for example in delta systems, tend to favour the formation of cyclic steps (Figs 7 and 8) (Dietrich *et al.*, 2016; Lang *et al.*, 2017b; Winsemann *et al.*, 2018), while gentler gradients, for example in glacifluvial systems or subaqueous (ice-contact) fans, are more prone to the formation of antidunes (Figs 2 and 6) (Russell & Arnott, 2003; Lang & Winsemann, 2013; Pisarska-Jamroży & Zieliński, 2014). The impacts of slope and flow confinement commonly act in conjunction, and slope breaks commonly also lead to a transition from confined to unconfined flows (Stacey *et al.*, 2019). Flow confinement impacts the run-out distance and competence of flows. Flows that leave a confined conduit are prone to dissipation due to rapid sediment deposition and water entrainment (Cartigny *et al.*, 2011; Hamilton *et al.*, 2015; Stacey *et al.*, 2019). In settings characterized by supercritical flows this leads to downflow transitions in bedform type and wavelength, and ultimately to a transition to subcritical flow conditions (Fedele *et al.*, 2016; Normandeau *et al.*, 2016; Stacey *et al.*, 2019). Based on previous field examples, Fedele *et al.* (2016) suggested that cyclic steps are more common in confined settings (i.e. channels), while antidunes prevail in non-confined settings (i.e. lobes). Observations from glacigenic successions support this idea. Cyclic-step deposits are common in more confined settings, such as the base of chutes, channels or incised valleys (Figs 5A and 9A) (Winsemann *et al.*, 2011; Lang & Winsemann, 2013; Winsemann *et al.*, 2018). Studies from modern delta systems suggest that cyclic steps preferentially form in channels on the delta slope (Hage *et al.*, 2018; Stacey *et al.*, 2019). Antidune deposits tend to dominate in unconfined settings, for example subaqueous aprons of ice-contact fans and lobes deposited by glacimarine density flows (Figs 8 and 11) (Hirst *et al.*, 2002; Hirst, 2012; Lang *et al.*, 2017b).

Sediment concentration and aggradation rate

Physical and numerical flow experiments have shown that the architecture and internal sedimentary structures of bedforms developed under supercritical flows depend on the sediment concentration, grain size and aggradation rate (Cartigny *et al.*, 2013, 2014; Vellinga *et al.*, 2018; Ono *et al.*, 2021). The effects of sediment concentration, grain size and aggradation rate may hamper the unambiguous recognition of bedforms at outcrop, as reflected by the broad range of sedimentary facies observed in glacigenic successions (Fig. 13), for example for deposits of cyclic steps and antidunes. Net-erosional bedforms may form during glacial lake-outburst floods under conditions of high discharge with comparatively low sediment availability or dominant bypass (Carling *et al.*, 2002, 2009; Johnsen & Brennand, 2004). Cyclic steps formed during the incision of valleys by lake-outburst floods or lake-level falls comprise laterally amalgamated or spaced scour fills (Lang & Winsemann, 2013; Winsemann *et al.*, 2016, 2018; Kostic *et al.*,

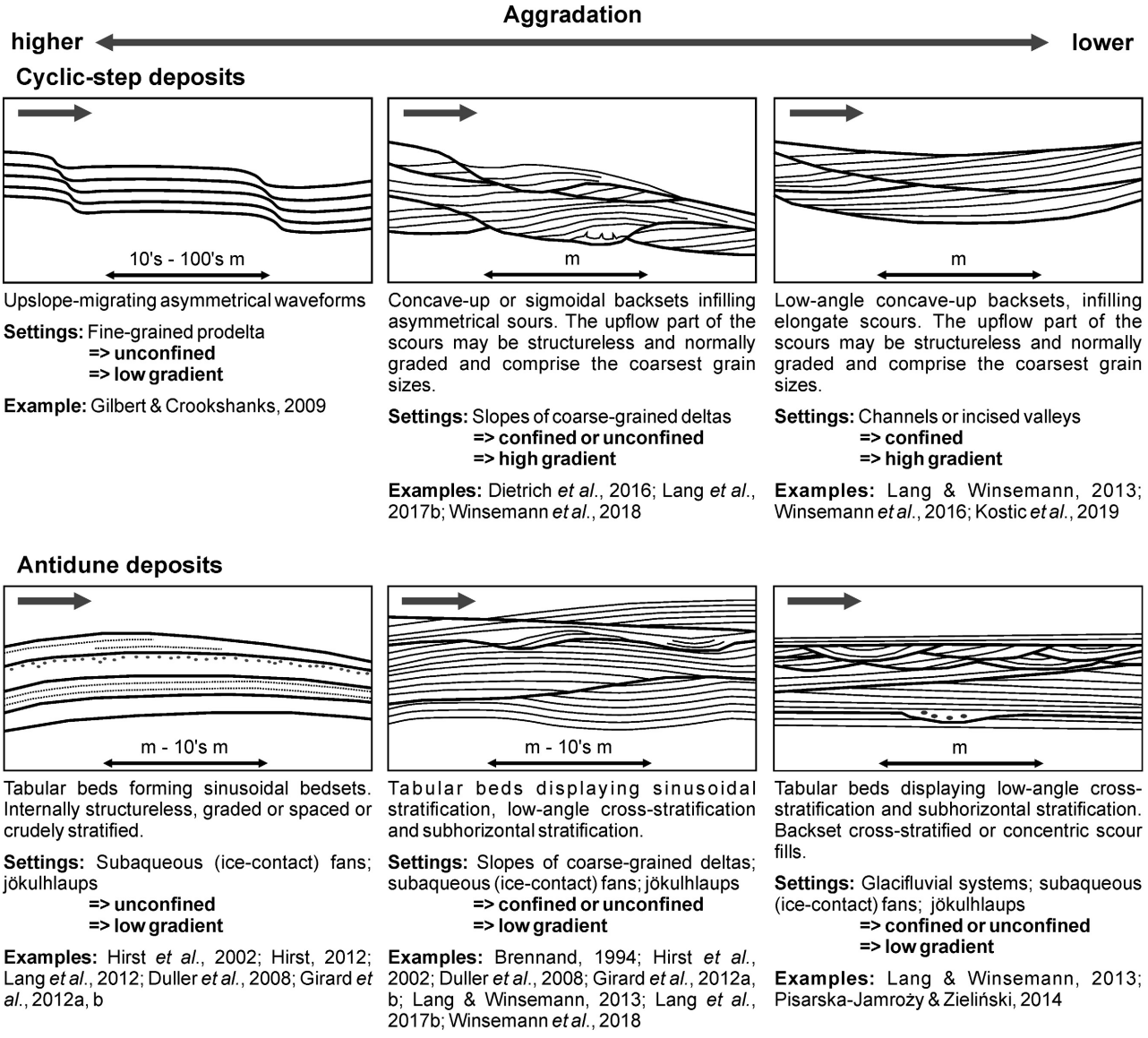

Fig. 13. Characteristic sedimentary structures of cyclic-step and antidune deposits formed under different aggradation rates.

2019), indicating the preservation of only the basal part of bedforms when aggradation rates are low (Fig. 13). Higher aggradation is documented by cyclic steps deposited on delta slopes, where trains of laterally stacked scour fills bear evidence of upslope migration (Dietrich *et al.*, 2016; Lang *et al.*, 2017b; Winsemann *et al.*, 2018). Repeated surveys of cyclic steps on a modern channelized glacifluvial delta slope suggest that only *ca* 11% of the bedform stratigraphy is preserved, while exceptionally high aggradation and preservation relate to less common delta-brink failures (Vendettuoli *et al.*, 2019). Gilbert & Crookshanks (2009) showed that preservation of complete cyclic-step bedforms may occur on fine-grained distal delta-slopes. These cyclic-step deposits resemble those deposited in deep marine settings under highly aggradational conditions (Cartigny *et al.*, 2011; Kostic, 2011; Symons *et al.*, 2016; Lang *et al.*, 2017a). Antidunes also produce a range of sedimentary structures under different aggradation rates. Low-angle backsets and shallow scour fills are deposited in glacifluvial systems during the melt season (Fig. 13) (Kjær *et al.*, 2004; Pisarska-Jamroży & Zieliński, 2014). These antidune deposits indicate rather low aggradation rates, although glacifluvial systems during the melt

season typically have comparatively high discharge and sediment concentration compared with other fluvial systems (Marren, 2005). In contrast, antidunes deposited by jökulhlaups (Duller *et al.*, 2008; Girard *et al.*, 2015) or subaqueous density flows (Brennand, 1994; Hirst, 2012; Lang & Winsemann, 2013; Lang *et al.*, 2017b; Winsemann *et al.*, 2018) comprise thickly bedded, sinusoidally stratified units (Fig. 13), where antidune waveforms are almost completely preserved. These deposits are similar to antidune successions deposited by highly aggradational turbidity currents (Ito & Saito, 2006; Ito, 2010; Lang *et al.*, 2017a; West *et al.*, 2019).

Different sediment concentrations and aggradation rates produce variable stratification styles. Well-developed internal lamination is the most common stratification style in glacigenic upper-flow-regime bedforms (Figs 4, 5C and 8C to E), indicating grain-by-grain bedload aggradation under turbulent low-density flows. The occurrence of spaced or crude stratification in some beds (Figs 4B, 7A, 7E, 7F and 11B) points to flows with higher sediment concentration (Cartigny *et al.*, 2013). These beds may display normal (Fig. 7A and F) or inverse (Fig. 8G) grading, the latter commonly attributed to traction carpets (cf. Hiscott, 1994; Sohn, 1997). However, antidune deposits may display highly variable stratification styles and many deposits attributed to traction carpets may relate to antidunes (Yagishita, 1994; Lang *et al.*, 2017a; Postma *et al.*, 2020). The occurrence of structureless, diffusely stratified and graded beds (Fig. 6C and D) points to deposition by concentrated flows (Russell & Arnott, 2003; Winsemann *et al.*, 2004, 2007a, 2009; Duller *et al.*, 2010) where the formation of stratification is suppressed by high sediment concentration (Arnott & Hand, 1989; Cartigny *et al.*, 2013). Structureless or normally graded scour fills (Figs 7A, 7D and 9B) are attributed to rapid suspension fall-out in the hydraulic-jump zones of cyclic steps or chutes-and-pools (Postma *et al.*, 2009; Postma & Cartigny, 2014; Lang *et al.*, 2017a,b; Winsemann *et al.*, 2018).

Sediment grain size

Bedform geometry and sedimentary facies in upper-flow-regime deposits are impacted by grain size (Cartigny *et al.*, 2014; Postma & Cartigny, 2014; Ono *et al.*, 2021). However, detailed studies of very fine-grained (i.e. mud-dominated; e.g. Gilbert & Crookshanks, 2009) and very coarse-grained (i.e. gravel-dominated; e.g. Brennand, 1994; Lang *et al.*, 2017b) bedforms are rare. The cyclic-step bedforms and depositional architecture preserved on a muddy glacilacustrine delta slope (Fig. 13) (Gilbert & Crookshanks, 2009) resemble those documented from deep marine settings (Cartigny *et al.*, 2011; Kostic, 2011; Symons *et al.*, 2016; Lang *et al.*, 2017a). Deposits comprising gravelly sediment tend to display steeper scour margins and backsets and a predominance of lenticular bed geometries with intense internal scouring (Fig. 7B to D) (Winsemann *et al.*, 2009; Lang *et al.*, 2017b). Steeper scour margins and backsets can be related to more rapid settling of coarser-grained clasts. The predominance of lenticular scour fills is caused by the stronger flows required to transport coarse-grained sediment and the lower threshold for antidune-wave breaking or hydraulic-jump formation in flows over hydraulically rough gravelly beds (Breakspear, 2008). The extreme end-member of coarse-grained sediment in combination with low aggradation is represented by the formation of transverse ribs. Transverse ribs, consisting of regularly spaced clusters of imbricated cobbles to boulders, have been described from modern glacifluvial systems (Gustavson, 1974) and are interpreted to form beneath antidune waves (Gustavson, 1974) or beneath trains of hydraulic jumps (Allen, 1983; Grant, 1997), similar to cyclic steps. The occurrence of imbricated gravel clusters on laterally continuous erosional surfaces (Winsemann *et al.*, 2009; Lang *et al.*, 2017b) indicates that transverse ribs are the first bedforms to be deposited after extensive scouring. The clustering of the gravel also hinders remobilization, favouring the preservation of these structures (Allen, 1983).

Discharge variations

Both in glacigenic and non-glacigenic depositional environments the formation and preservation of upper-flow-regime bedforms and sedimentary structures are commonly attributed to discharge variations, especially to high-magnitude flood events. Such discharge variations may affect all studied sub-environments of deposition.

In subaerial settings upper-flow-regime bedforms generally record high-discharge events and/or high discharge variations during the melt season (Kjær *et al.*, 2004; Pisarska-Jamroży & Zieliński, 2014), jökulhlaups (Burke *et al.*, 2008, 2010a,b; Duller *et al.*, 2008; Girard *et al.*, 2015) or the catastrophic drainage of proglacial lakes

(Johnsen & Brennand, 2004; Winsemann *et al.*, 2011, 2016; Lang & Winsemann, 2013; Hansen *et al.*, 2020). High rates of aggradation under supercritical flows in subaerial glacigenic deposits allow for the more complete preservation of bedforms in thicker successions than those in other types of fluvial systems (Alexander & Fielding, 1997; Fielding *et al.*, 2010; Froude *et al.*, 2017).

Deposits of subaqueous supercritical density flows are also commonly attributed to high-discharge events (Russell & Arnott, 2003; Winsemann *et al.*, 2009; Girard *et al.*, 2012a,b; Lang *et al.*, 2017b). In some field examples, jökulhlaup deposits that include sedimentary structures related to supercritical flows could be laterally traced from delta-plain into delta-slope deposits (Girard *et al.*, 2012a,b). Observations from modern systems demonstrate that supercritical density flows on a delta slope are triggered on a daily basis from low-density river plumes, and high-discharge events are not a prerequisite (Hage *et al.*, 2018; Hizzett *et al.*, 2018; Vendettuoli *et al.*, 2019). Less common high-magnitude events have far longer run-out distances and supply large amounts of sediment that may partly be redistributed by subsequent lower-magnitude flows (Stacey *et al.*, 2019; Vendettuoli *et al.*, 2019). Many glacilacustrine and glacimarine successions deposited by supercritical density flows display coarse-grained sediment and high thickness, which can more easily be explained by aggradation during high-discharge events. Dowdeswell *et al.* (2015) pointed out that the deposition of large subaqueous ice-contact fans and thick underflow deposits requires higher discharges, flow velocities and sediment concentrations than those measured in modern systems.

Flow parameters during high-discharge events, like flow velocity and inundation depth, can be estimated from the dimensions of the preserved upper-flow-regime bedforms (Duller *et al.*, 2008; Winsemann *et al.*, 2011). Such quantitative estimates are straightforward in subaerial settings, where bedform wavelength can be directly linked to the flow velocity and depth (Duller *et al.*, 2008; Froude *et al.*, 2017). For bedforms deposited by density flows in subaqueous settings such quantitative estimates need to be handled more carefully. In subaqueous density flows, the excess density of the flow compared with the ambient fluid has to be considered when calculating flow parameters from bedform dimensions (Hand, 1974; Fedele *et al.*, 2016). However, the flow density is very hard to estimate from the depositional record. Furthermore, in many cases (especially high-density flows) a calculated flow depth may only be representative for the dense basal layer of a flow (cf. Postma *et al.*, 1988; Postma & Cartigny, 2014).

CONCLUSIONS

Upper-flow-regime bedforms are ubiquitous in glacigenic depositional environments. A review of the existing literature shows that several studies have presented detailed analyses of upper-flow-regime bedforms and sedimentary facies architecture, as well as numerous studies that simply noted the occurrence of deposits attributed to supercritical flows.

Deposits of upper-stage-plane beds, antidunes, chutes-and-pools and cyclic steps are known from all kinds of glacigenic depositional systems, and typically are indicative of ice-proximal settings and/or high-discharge events. The bedforms can develop in subglacial, subaerial and subaqueous environments, recording deposition by both open-channel flows and submerged density flows. In addition to modern and Pleistocene records, upper-flow-regime bedforms are increasingly recognized from Palaeozoic (particularly Late Ordovician, and to a lesser extent Permo-Carboniferous) glacigenic deposits.

This review implies that the bedforms and bedform successions are generally not specific for any glacigenic depositional environment, and that very similar successions are documented from all sub-environments. Lateral and vertical trends in bedform distribution are similar to those in non-glacigenic settings. Important controlling factors for bedform evolution that differ between depositional environments include the degree of flow confinement, gradient of the depositional surface, sediment concentration, grain size and aggradation rate. Deposits of cyclic steps are more common in confined settings or on steeper slopes, for example in channels or incised valleys or along the foresets of glacifluvial deltas. In contrast, antidune deposits dominate in unconfined settings, like glacifluvial fans or subaqueous (ice-contact) fans.

Differences in bedform architecture and the resulting sedimentary facies and stratification styles are affected by different sediment concentration, aggradation rate and grain size, as demonstrated by previous physical and

numerical experiments (e.g. Cartigny *et al.*, 2013, 2014; Vellinga *et al.*, 2018). Under low aggradation rates, only the basal parts of bedforms are preserved, for example scour fills formed in the hydraulic-jump zone of cyclic steps or by antidune-wave breaking. Low aggradation rates are common in glacifluvial systems and during the erosional phase of glacial lake-outburst floods and lake-level falls. Higher rates of aggradation result in increased bedform preservation, potentially allowing for the preservation of complete bedform trains under particularly high aggradation rates. Such conditions are met for example in sediment-laden jökulhlaups and subaqueous environments characterized by expanding density flows. Coarser-grained deposits are characterized by steeper bedforms and sedimentary structures and by highly scoured facies architectures, while finer-grained deposits display more gently dipping stratal surfaces. The differences are caused by stronger flows, faster settling of coarse-grained sediment and more rapid antidune wave-breaking/hydraulic jump formation over rougher beds.

The wavelengths of upper-flow-regime bedforms can be used to estimate flow parameters, like flow velocity and inundation depth, especially during high-discharge events. These estimations are straightforward in subaerial settings, where bedform wavelength can be directly linked to flow depth and velocity. In subaqueous settings, the flow density is another necessary parameter, yet one that is commonly hard to estimate accurately. Therefore, a careful consideration of the depositional environment is required if flow parameters are to be quantified based on sedimentary structures.

ACKNOWLEDGEMENTS

Open access funding provided by Projekt DEAL. We would like to thank the editorial team (A. Slootman, M. Cartigny, A. Normandeau, D. Ventra and S. Hubbard) of the *Sedimentology* special issue for inviting us to contribute this paper. Discussions on bedform morphodynamics with J. Fedele, D. Hoyal and G. Postma helped to sharpen our ideas. T. Hartmann helped with artwork. Special thanks go to the owners of the open-pits for the permission to work on their properties and R. Duller, M. Pisarska-Jamroży and T. Zieliński for sharing outcrop photographs. Constructive reviews by P. Carling, R. Duller and D. Ventra are highly appreciated.

DATA AVAILABILITY STATEMENT

The data that support the findings of this study are available from the corresponding author upon reasonable request.

REFERENCES

Ahokangas, E. and **Mäkinen, J.** (2014) Sedimentology of an ice lobe margin esker with implications for the deglacial dynamics of the Finnish Lake District lobe trunk. *Boreas*, **43**, 90–106.

Alexander, J. and **Fielding, C.** (1997) Gravel antidunes in the tropical Burdekin River, Queensland, Australia. *Sedimentology*, **44**, 327–337.

Alexander, J., **Bridge, J.S.**, **Cheel, R.J.** and **Leclair, S.F.** (2001) Bedforms and associated sedimentary structures formed under supercritical water flows over aggrading sand beds. *Sedimentology*, **48**, 133–152.

Alho, P., **Baker, V.R.** and **Smith, L.N.** (2010) Paleohydraulic reconstruction of the largest Glacial Lake Missoula draining(s). *Quat. Sci. Rev.*, **29**, 3067–3078.

Allen, J.R.L. (1983) A simplified cascade model for transverse stone-ribs in gravelly streams. *Proc. R. Soc. Lond. A*, **385**, 253–266.

Allen, J.R.L. (1984) Sedimentary structures: their character and physical basis. *Dev. Sedimentol.*, **30**, 1–663.

Alonso-Muruaga, P.J., **Limarino, C.O.**, **Spalletti, L.A.** and **Piñol, F.C.** (2018) Depositional settings and evolution of a fjord system during the carboniferous glaciation in Northwest Argentina. *Sed. Geol.*, **369**, 28–45.

Aquino, C.D., **Buso, V.V.**, **Faccini, U.F.**, **Milana, J.P.** and **Paim, P.S.G.** (2016) Facies and depositional architecture according to a jet efflux model of a late Paleozoic tidewater grounding-line system from the Itararé Group (Paraná Basin), southern Brazil. *J. S. Am. Earth Sci.*, **67**, 180–200.

Arnaud, E., **Halverson, G.P.** and **Shields-Zhou, G.** (Eds). (2011) *The Geological Record of Neoproterozoic Glaciations. Geol. Soc. Mem.*, **36**, 735 pp.

Arnott, R.W.C. and **Hand, B.M.** (1989) Bedforms, primary structures and grain fabric in the presence of suspended sediment rain. *J. Sed. Res.*, **59**, 1062–1069.

Ashley, G.M. (1995) Glaciolacustrine environments. In: *Modern Glacial Environments* (Ed. Menzies, J.), pp. 417–444 Butterworth-Heinemann, Oxford.

Assine, M.L., **de Santa Ana, H.**, **Veroslavsky, G.** and **Vesely, F.F.** (2018) Exhumed subglacial landscape in Uruguay: Erosional landforms, depositional environments, and paleo-ice flow in the context of the late Paleozoic Gondwanan glaciation. *Sed. Geol.*, **369**, 1–12.

Bache, F., **Moreau, J.**, **Rubino, J.-L.**, **Gorini, C.** and **Van-Vliet Lanoë, B.** (2012) The subsurface record of the Late Palaeozoic glaciation in the Chaco Basin, Bolivia. *Geol. Soc. London, Spec. Pub.*, **368**(1), 257–274.

Baker, V.R. (1973) Paleohydrology and sedimentology of Lake Missoula flooding in eastern Washington. *Geol. Soc. Am. Spec. Pap.*, **144**, 1–79.

Banerjee, I. and **McDonald, B.C.** (1975). Nature of esker sedimentation. In: *Glaciofluvial and Glaciolacustrine Sedimentation* (Eds Jopling, A.V. and McDonald, B.C.), *SEPM Spec. Pub.*, **23**, 304–320.

Bataller, F.J., **McDougall, N.** and **Moscariello, A.** (2019) Ordovician glacial paleogeography. Integration of seismic spectral decomposition, well sedimentological data and glacial modern analogues in the Murzuq Basin, Libya. *Interpretation*, **7**, 1–26.

Bates, C.C. (1953) Rational theory of delta formation. *AAPG Bul.*, **37**, 2119–2162.

Best, J. and **Bridge, J.** (1992) The morphology and dynamics of low amplitude bedwaves upon upper stage plane beds and the preservation of planar laminae. *Sedimentology*, **39**, 737–752.

Blair, T.C. (1999) Sedimentary processes and facies of the waterlaid Anvil Spring Canyon alluvial fan, Death Valley, California. *Sedimentology*, **46**, 913–940.

Blažauskas, N., **Jurgaitis, A.** and **Šinkūnas, P.** (2007) Patterns of Late Pleistocene proglacial fluvial sedimentation in the SE Lithuanian Plain. *Sed. Geol.*, **193**, 193–201.

Bohorquez, P., **Carling, P.A.** and **Herget, J.** (2016) Dynamic simulation of catastrophic late Pleistocene glacial-lake drainage, Altai Mountains, central Asia. *Int. Geol. Rev.*, **58**, 1795–1817.

Breakspear, R. (2008) *Hydrodynamics and Sedimentary Structures of Antidunes in Gravel and Sand Mixtures*. PhD thesis. University of Southampton, Southampton, 355 pp.

Brennand, T.A. (1994) Macroforms, large bedforms and rhythmic sedimentary sequences in subglacial eskers, south-central Ontario: implications for esker genesis and meltwater regime. *Sed. Geol.*, **91**, 9–55.

Brennand, T.A. and **Shaw, J.** (1996) The Harricana glaciofluvial complex, Abitibi region, Quebec: its genesis and implications for meltwater regime and ice-sheet dynamics. *Sed. Geol.*, **102**, 221–262.

Bridge, J.S. and **Best, J.L.** (1988) Flow, sediment transport and bedform dynamics over the transition from dunes to upper-stage plane beds: implications from the formation of planar laminae. *Sedimentology*, **35**, 753–763.

Burke, M.J., **Woodward, J.**, **Russell, A.J.**, **Fleisher, P.J.** and **Bailey, P.K.** (2008) Controls on the sedimentary architecture of a single event englacial esker: Skeiðarárjökull, Iceland. *Quatern. Sci. Rev.*, **27**, 1829–1847.

Burke, M.J., **Woodward, J.** and **Russell, A.J.** (2010a) Sedimentary architecture of large-scale, jökulhlaup-generated, ice-block obstacle marks: Examples from Skeiðarársandur, SE Iceland. *Sed. Geol.*, **227**, 1–10.

Burke, M.J., **Woodward, J.**, **Russell, A.J.**, **Fleisher, P.J.** and **Bailey, P.K.** (2010b) The sedimentary architecture of outburst flood eskers: a comparison of ground-penetrating radar data from Bering Glacier, Alaska and Skeiðarárjökull, Iceland. *GSA Bul.*, **122**, 1637–1645.

Busfield, M.E. and **Le Heron, D.P.** (2016) A Neoproterozoic ice advance sequence, Sperry Wash, California. *Sedimentology*, **63**, 307–330.

Bussert, R. (2014) Depositional environments during the Late Palaeozoic ice age (LPIA) in northern Ethiopia, NE Africa. *J. Afr. Earth Sci.*, **99**, 386–407.

Carling, P.A. (2013) Freshwater megaflood sedimentation: What can we learn about generic processes? *Earth-Sci. Rev.*, **125**, 87–113.

Carling, P.A. and **Leclair, S.F.** (2019) Alluvial stratification styles in a large, flash-flood influenced dryland river: The Luni River, Thar Desert, north-west India. *Sedimentology*, **66**, 102–128.

Carling, P.A., **Kirkbride, A.D.**, **Parnachov, S.**, **Borodavko, P.S.** and **Berger, G.W.** (2002) Late Quaternary catastrophic flooding in the Altai Mountains of south-central Siberia: a synoptic overview and an introduction to flood deposit sedimentology. In: *Flood and Megaflood Processes and Deposits* (Ed. Martini, P.), *Spec. Publ. Int. Assoc. Sedimentol.*, **32**, 17–35.

Carling, P.A., **Burr, D.M.**, **Johnsen, T.F.** and **Brennand, T.A.** (2009) A review of open-channel megaflood depositional landforms on Earth and Mars. In: *Megaflooding on Earth and Mars* (Eds Burr, D.M., Carling, P.A. and Baker, V.R.), pp. 33–49. Cambridge University Press, Cambridge.

Carrivick, J.L. (2006) Application of 2D hydrodynamic modelling to high-magnitude outburst floods: an example from Kverkfjöll, Iceland. *J. Hydrol.*, **321**, 187–199.

Cartigny, M.J.B. and **Postma, G.** (2016) Turbidity current bedforms. In: *Atlas of Bedforms in the Western Mediterranean* (Eds Guillén, J., Acosta, J., Palanques, A. and Chiocci, F.L.), pp. 29–33. Springer, Heidelberg.

Cartigny, M.J.B., **Postma, G.**, **Van den Berg, J.H.** and **Mastbergen, D.** (2011) A Comparative study of sediment waves and cyclic steps based on geometries, internal structures and numerical modelling. *Mar. Geol.*, **280**, 40–56.

Cartigny, M.J.B., **Eggenhuisen, J.T.**, **Hansen, E.W.** and **Postma, G.** (2013) Concentration-dependent flow stratification in experimental high-density turbidity currents and their relevance to turbidite facies models. *J. Sed. Res.*, **83**, 1046–1064.

Cartigny, M.J.B., **Ventra, D.**, **Postma, G.** and **Van den Berg, J.H.** (2014) Morphodynamics and sedimentary structures of bedforms under supercritical-flow conditions: new insights from flume experiments. *Sedimentology*, **61**, 712–748.

Carvalho, A.H. and **Vesely, F.F.** (2017) Facies relationships recorded in a Late Paleozoic fluvio-deltaic system (Paraná Basin, Brazil): Insights into the timing and triggers of subaqueous sediment gravity flows. *Sed. Geol.*, **352**, 45–62.

Chakraborty, C. and **Bose, P.K.** (1992) Ripple/dune to upper stage plane bed transition: some observations from the ancient record. *Geol. J.*, **27**, 349–359.

Chu, V.W. (2014) Greenland ice sheet hydrology: A review. *Prog. Phys. Geogr.*, **38**, 19–54.

Clemmensen, L.B. and **Houmark-Nielsen, M.** (1981) Sedimentary features of a Weichselian glaciolacustrine delta. *Boreas*, **10**, 229–245.

Covault, J.A., **Kostic, S.**, **Paull, C.K.**, **Sylvester, Z.** and **Fildani, A.** (2017) Cyclic steps and related supercritical bedforms: building blocks of deep-water depositional systems, western North America. *Mar. Geol.*, **393**, 4–20.

Cuffey, K.M. and **Paterson, W.S.B.** (2010) *The Physics of Glaciers*. Elsevier, Amsterdam, 693 pp.

Dabrio, C., **Bardají, T.**, **Zazo, C.** and **Goy, J.I.** (1991) Effects of sea-level changes on a wave-worked Gilbert-type delta (Late Pliocene, Aguilas Basin, SE Spain). *Cuadernos de Geol. Ibérica*, **15**, 103–137.

Deschamps, R., **Eschard, R.** and **Roussé, S.** (2013) Architecture of Late Ordovician glacial valleys in the Tassili N'Ajjer area (Algeria). *Sed. Geol.*, **289**, 124–147.

Di Celma, C., **Pitts, A.**, **Jablonská, D.** and **Haynes, J.T.** (2020) Backset lamination produced by supercritical backwash flows at the beachface-shoreface transition of a storm-dominated gravelly beach (middle Pleistocene, central Italy). *Mar. Petrol. Geol.*, **112**, 103987.

Dietrich, P. and **Hofmann, A.** (2019) Ice-margin fluctuation sequences and grounding zone wedges: the record of the Late Palaeozoic Ice Age in the eastern Karoo Basin (Dwyka Group, South Africa). *Deposit. Rec.*, **5**, 247–271.

Dietrich, P., **Ghienne, J.-F.**, **Normandeau, A.** and **Lajeunesse, P.** (2016) Upslope-migrating bedforms in a proglacial sandur delta: cyclic steps from river-derived underflows? *J. Sed. Res.*, **86**, 113–123.

Dietrich, P., **Ghienne, J.F.**, **Schuster, M.**, **Lajeunesse, P.**, **Nutz, A.**, **Deschamps, R.**, **Roquin, C.** and **Duringer, P.** (2017) From outwash to coastal systems in the Portneuf-Forestville deltaic complex (Quebec North Shore): Anatomy of a forced regressive deglacial sequence. *Sedimentology*, **64**, 1044–1078.

Dietrich, P., **Ghienne, J.F.**, **Lajeunesse, P.**, **Normandeau, A.**, **Deschamps, R.** and **Razin, P.** (2019) Deglacial sequences and glacio-isostatic adjustment: Quaternary compared with Ordovician glaciations. *Geol. Soc. London, Speci. Pub.*, **475**(1), 149–179.

Dowdeswell, J.A., **Hogan, K.A.**, **Arnold, N.S.**, **Mugford, R.I.**, **Wells, M.**, **Hirst, J.P.P.** and **Decalf, C.** (2015) Sediment-rich meltwater plumes and ice-proximal fans at the margins of modern and ancient tidewater glaciers: Observations and modelling. *Sedimentology*, **62**, 1665–1692.

Duller, R.A., **Mountney, N.P.**, **Russell, A.J.** and **Cassidy, N.C.** (2008) Architectural analysis of a volcaniclastic jökulhlaup deposit, southern Iceland: sedimentary evidence for supercritical flow. *Sedimentology*, **55**, 939–964.

Duller, R.A., **Mountney, N.P.** and **Russell, A.J.** (2010) Particle fabric and sedimentation of structureless sand, Southern Iceland. *J. Sed. Res.*, **80**, 562–577.

Duller, R.A., **Warner, N.H.**, **De Angelis, S.**, **Armitage, J.J.** and **Poyatos-Moré, M.** (2015) Reconstructing the timescale of a catastrophic fan-forming event on Earth using a Mars model. *Geophys. Res. Let.*, **42**, 10324–10332.

Eyles, N. (2008) Glacio-epochs and the supercontinent cycle after $\sim$ 3.0 Ga: tectonic boundary conditions for glaciation. *Palaeogeogr. Palaeoclimatol. Palaeoecol.*, **258**, 89–129.

Eyles, N. and **Januszczak, N.** (2004) 'Zipper-rift': a tectonic model for Neoproterozoic glaciations during the breakup of Rodinia after 750 Ma. *Earth-Sci. Rev.*, **65**, 1–73.

Fedele, J.J., **Hoyal, D.C.**, **Barnaal, Z.**, **Tulenko, J.** and **Awalt, S.** (2016) Bedforms created by gravity flows. In:*Autogenic Dynamics In Sedimentary Systems*(EdsBudd, D., Hajek, E. and Purkis, S.), *SEPM Spec. Publ.*, **106**, 95–121.

Fielding, C.R. (2006) Upper flow regime sheets, lenses and scour fills: Extending the range of architectural elements for fluvial sediment bodies. *Sed. Geol.*, **190**, 227–240.

Fielding, C.R., **Frank, T.D.**, **Isbell, J.L.**, **Henry, L.C.** and **Domack, E.W.** (2010) Stratigraphic signature of the late Paleozoic Ice Age in the Parmeener Supergroup of Tasmania, SE Australia, and inter-regional comparisons. *Palaeogeogr. Palaeoclimatol. Palaeoecol.*, **298**, 79–90.

Fiore, J., **Pugin, A.** and **Beres, M.** (2002) Sedimentological and GPR studies of subglacial deposits in the Joux Valley (Vaud, Switzerland): backset accretion in an esker followed by an erosive jökulhlaup. *Géog. Phys. Quatern.*, **56**, 19–32.

Fisher, T.G., **Taylor, L.D.** and **Jol, H.M.** (2003) Boulder-gravel hummocks and wavy basal till contacts: products of subglacial meltwater flow beneath the Saginaw Lobe, south-central Michigan, USA. *Boreas*, **32**, 328–336.

Froude, M.J., **Alexander, J.**, **Barclay, J.** and **Cole, P.** (2017) Interpreting flash flood palaeoflow parameters from antidunes and gravel lenses: An example from Montserrat, West Indies. *Sedimentology*, **64**, 1817–1845.

Ghienne, J.-F., **Girard, F.**, **Moreau, J.** and **Rubino, J.-L.** (2010) Late Ordovician climbing-dune cross-stratification: a signature of outburst floods in proglacial outwash environments? *Sedimentology*, **57**, 1175–1198.

Gilbert, G.K. (1914) The transportation of débris by running water. *US Geol. Surv. Prof. Pap.*, **86**, 263 pp.

Gilbert, R. and **Crookshanks, S.** (2009) Sediment waves in a modern high-energy glacilacustrine environment. *Sedimentology*, **56**, 645–659.

Girard, F., **Ghienne, J.F.** and **Rubino, J.L.** (2012a) Channelized sandstone bodies ('cordons') in the Tassili N'Ajjer (Algeria & Libya): snapshots of a Late Ordovician proglacial outwash plain. In: *Glaciogenic Reservoirs* (Eds Huuse, M., Redfern, J., Le Heron, D.P., Dixon, R.J., Moscariello, A. and Craig, J.), *Geol. Soc. Spec. Pub.*, **368**, 355–379.

Girard, F., **Ghienne, J.** and **Rubino, J.L.** (2012b) Occurrence of hyperpyncal flows and hybrid event beds related to glacial outburst events in a Late Ordovician proglacial delta (Murzuq Basin, SW Libya. *J. Sed. Res.*, **82**, 688–708.

Girard, F., **Ghienne, J. F.**, **Du-Bernard, X.** and **Rubino, J. L.** (2015) Sedimentary imprints of former ice-sheet margins: Insights from an end-Ordovician archive (SW Libya). *Earth-Sci. Rev.*, **148**, 259–289.

Gobo, K., **Ghinassi, M.** and **Nemec, W.** (2014) Reciprocal changes in foreset to bottomset facies in a Gilbert-type delta: response to short-term changes in base level. *J. Sed. Res.*, **84**, 1079–1095.

Gobo, K., **Ghinassi, M.** and **Nemec, W.** (2015) Gilbert-type deltas recording short-term base-level changes: Delta-brink morphodynamics and related foreset facies. *Sedimentology*, **62**, 1923–1949.

Gorrell, G. and **Shaw, J.** (1991) Deposition in an esker, bead and fan complex, Lanark, Ontario, Canada. *Sed. Geol.*, **72**, 285–314.

Grant, G.E. (1997) Critical flow constrains flow hydraulics in mobile-bed streams: A new hypothesis. *Water Resour. Res.*, **33**, 349–358.

Gupta, S., **Collier, J.S.**, **Palmer-Felgate, A.** and **Potter, G.** (2007) Catastrophic flooding origin of shelf valley systems in the English Channel. *Nature*, **448**, 342–345.

Gupta, S., **Collier, J.S.**, **Garcia-Moreno, D.**, **Oggioni, F.**, **Trentesaux, A.**, **Vanneste, K.**, **De Batst, M.**, **Camelbeeck, T.**, **Potter, G.**, **Van Vliet-Lanoë, B.** and **Arthur, J.C.** (2017) Two-stage opening of the Dover Strait and the origin of island Britain. *Nature Comm.*, **8**, 15101.

Gustavson, T.C. (1974) sedimentation on gravel outwash fans, Malaspina glacier foreland, Alasaka. *J. Sed. Petrol.*, **44**, 374–389.

Hage, S., **Cartigny, M.J.B.**, **Clare, M.A.**, **Sumner, E.J.**, **Vendettuoli, D.**, **Hughes Clarke, J.E.**, **Hubbard, S.M.**, **Talling, P.J.**, **Gwyn Lintern, D.**, **Englert, R.G.**, **Vardy, M.E.**, **Hunt, J.E.**, **Yokokawa, M.**, **Parsons, D.R.**, **Hizzett, J.L.**, **Azpiroz-Zabala, M.** and **Vellinga, A.J.** (2018) How to recognize crescentic bedforms formed by supercritical turbidity currents in the geologic record: Insights from active submarine channels. *Geology*, **46**, 563–566.

Hage, S., **Cartigny, M.J.B.**, **Sumner, E.J.**, **Clare, M.A.**, **Hughes Clarke, J.E.**, **Talling, P.J.**, **Gwyn Lintern, D.**, **Simmons, S.M.**, **Jacinto, R.S.**, **Vellinga, A.J.**, **Allin, J.R.**, **Azpiroz-Zabala, M.**, **Gales, J.A.**, **Hizzett, J.L.**, **Hunt, J.E.**, **Mozzato, A.**, **Parsons, D.R.**, **Pope, E.L.**, **Stacey, C.D.**, **Symons, W.O.**, **Vardy, M.E.** and **Watts, C.** (2019) Direct monitoring

reveals initiation of turbidity currents from extremely dilute river plumes. *Geophys. Res. Lett.*, **46**, 11310–11320.

Hamilton, P.B., **Strom, K.B.** and **Hoyal, D.C.** (2015) Hydraulic and sediment transport properties of autogenic avulsion cycles on submarine fans with supercritical distributaries. *J. Geophys. Res. Earth Surf.*, **120**, 1369–1389.

Hanáček, M., **Nývlt, D.**, **Skácelová, Z.**, **Nehyba, S.**, **Procházková, B.** and **Engel, Z.** (2018) Sedimentary evidence for an ice-sheet dammed lake in a mountain valley of the Eastern Sudetes, Czechia. *Geol. Pol.*, **68**, 107–134.

Hand, B.M. (1974) Supercritical flow in density currents. *J. Sed. Petrol.*, **44**, 637–648.

Hansen, L., **Tassis, G.** and **Høgaas, F.** (2020) Sand dunes and valley fills from Preboreal glacial-lake outburst floods in south-eastern Norway – beyond the aeolian paradigm. *Sedimentology*, **67**, 810–848.

Herget, J. (2005) Reconstruction of Pleistocene ice-dammed lake outburst floods in the Altai-Mountains, Siberia. *Geol. Soc. Am. Spec. Pap.*, **386**, 1–118.

Herget, J., **Euler, T.**, **Roggenkamp, T.** and **Zemke, J.** (2013) Obstacle marks as palaeohydraulic indicators of Pleistocene megafloods. *Hydrol. Res.*, **44**, 300–317.

Hirst, J.P.P. (2012) Ordovician proglacial sediments in Algeria: insights into the controls on hydrocarbon reservoirs in the In Amenas field, Illizi Basin. *Geol. Soc., London, Spec. Pub.*, **368**(1), 319–353.

Hirst, J.P.P., **Benbakir, A.**, **Payne, D.F.** and **Westlake, I.R.** (2002) Tunnel valleys and density flow processes in the Upper Ordovician glacial succession, Illizi Basin, Algeria: influence on reservoir quality. *J. Petrol. Geol.*, **25**, 297–324.

Hiscott, R.N. (1994) Traction-carpet stratification in turbidites-fact or fiction? *J. Sed. Res.*, **64**, 204–208.

Hizzett, J.L., **Hughes Clarke, J.E.**, **Sumner, E.J.**, **Cartigny, M.J.B.**, **Talling, P.J.** and **Clare, M.A.** (2018) Which triggers produce the most erosive, frequent, and longest runout turbidity currents on deltas? *Geophys. Res. Lett.*, **45**, 855–863.

Hornung, J.J., **Asprion, U.** and **Winsemann, J.** (2007) Jet-efflux deposits of a subaqueous ice-contact fan, glacial Lake Rinteln, northwestern Germany. *Sed. Geol.*, **193**, 167–192.

Hoyal, D.C.J.D., **Van Wagoner, J.C.**, **Adair, N.L.**, **Deffenbaugh, M.**, **Li, D.**, **Sun, T.**, **Huh, C.** and **Griffin, D.E.** (2003) Sedimentation from Jets: A Depositional Model for Clastic Deposits of all Scales and Environments. Search and Discovery Article 40082 (Online-Journal; AAPG/Datapages, Inc., 1444 South Boulder, Tulsa, OK, 74119, USA).

Hughes Clarke, J.E.H. (2016) First wide-angle view of channelized turbidity currents links migrating cyclic steps to flow characteristics. *Nature Comm.*, **7**, 11896.

Ito, M. (2010) Are coarse-grained sediment waves formed as downstream-migrating antidunes? Insight from an early Pleistocene submarine canyon on the Boso Peninsula, Japan. *Sed. Geol.*, **226**, 1–8.

Ito, M. and **Saito, T.** (2006) Gravel waves in an ancient canyon: analogous features and formative processes of coarse-grained bedforms in a submarine-fan system, the Lower Pleistocene of the Boso Peninsula, Japan. *J. Sed. Res.*, **76**, 1274–1283.

Izumi, N., **Yokokawa, M.** and **Parker, G.** (2017) Incisional cyclic steps of permanent form in mixed bedrock-alluvial rivers. *J. Geophys. Res.: Earth Surf.*, **122**, 130–152.

Janszen, A., **Moreau, J.**, **Moscariello, A.**, **Ehlers, J.** and **Kröger, J.** (2013) Time-transgressive tunnel-valley infill revealed by a three-dimensional sedimentary model, Hamburg, north-west Germany. *Sedimentology*, **60**, 693–719.

Johnsen, T.F. and **Brennand, T.A.** (2004) Late-glacial lakes in the Thompson Basin, British Columbia: paleogeography and evolution. *Can. J. Earth Sci.*, **41**, 1367–1383.

Kehew, A.E., **Piotrowski, J.A.** and **Jørgensen, F.** (2012) Tunnel valleys: Concepts and controversies – A review. *Earth-Sci. Rev.*, **113**, 33–58.

Kennedy, J.F. (1963) The mechanics of dunes and antidunes in erodible-bed channels. *J. Fluid. Mech.*, **16**, 521–544.

Kjær, K.H., **Sultan, L.**, **Krüger, J.** and **Schomacker, A.** (2004) Architecture and sedimentation of outwash fans in front of the Mýrdalsjökull ice cap, Iceland. *Sed. Geol.*, **172**, 139–163.

Koller, D., **Manica, R.**, **Borges, A.D.O.** and **Fedele, J.J.** (2019) Experimental bedforms by saline density currents. *Braz. J. Geol.*, **49**, 1–10.

Komar, P.D. (1971) Hydraulic jumps is turbidity currents. *Geol. Soc. Am. Bull.*, **82**, 1477–1488.

Kostic, S. (2011) Modeling of submarine cyclic steps: Controls on their formation, migration, and architecture. *Geosphere*, **7**, 294–304.

Kostic, S. (2014) Upper flow regime bedforms on levees and continental slopes: Turbidity current flow dynamics in response to fine-grained sediment waves. *Geosphere*, **10**, 1094–1103.

Kostic, S., **Casalbore, D.**, **Chiocci, F.**, **Lang, J.** and **Winsemann, J.** (2019) Role of upper-flow-regime bedforms emplaced by sediment gravity flows in the evolution of deltas. *J. Mar. Sci. Eng.*, **7**, 5. https://doi.org/10.3390/jmse7010005.

Krzyszkowski, D. (2002) Sedimentary successions in ice-marginal fans of the Late Saalian glaciation, southwestern Poland. *Sed. Geol.*, **149**, 93–109.

Lajeunesse, P. and **Allard, M.** (2002) Sedimentology of an ice-contact glaciomarine fan complex, Nastapoka Hills, eastern Hudson Bay, northern Québec. *Sed. Geol.*, **152**, 201–220.

Lang, J. and **Winsemann, J.** (2013) Lateral and vertical facies relationships of bedforms deposited by aggrading supercritical flows: from cyclic steps to humpback dunes. *Sed. Geol.*, **296**, 36–54.

Lang, J., **Fedele, J.J.** and **Hoyal, D.C.J.D.** (in review) Three-dimensional submerged wall jets and their transition to density flows – morphodynamics and implications for the depositional record. *Sedimentology*.

Lang, J., **Dixon, R.J.**, **Le Heron, D.P.** and **Winsemann, J.** (2012) Depositional architecture and sequence stratigraphic correlation of Upper Ordovician glacigenic deposits, Illizi Basin, Algeria. In: *Glaciogenic Reservoirs* (Eds Huuse, M., Redfern, J., Le Heron, D.P., Dixon, R.J., Moscariello, A. and Craig, J.), *Geol. Soc. Spec. Pub.*, **368**, 293–317.

Lang, J., **Brandes, C.** and **Winsemann, J.** (2017a) Erosion and deposition by supercritical density flows during channel avulsion and backfilling: Field examples from coarse-grained deepwater channel-levée complexes (Sandino Forearc Basin, southern Central America). *Sed. Geol.*, **349**, 79–102.

Lang, J., **Sievers, J.**, **Loewer, M.**, **Igel, J.** and **Winsemann, J.** (2017b) 3D architecture of cyclic-step and antidune deposits in glacigenic subaqueous fan and delta settings:

Integrating outcrop and ground-penetrating radar data. *Sed. Geol.*, **362**, 83–100.

Lang, J., **Alho, P.**, **Kasvi, E.**, **Goseberg, N.** and **Winsemann, J.** (2019) Impact of Middle Pleistocene (Saalian) glacial lake-outburst floods on the meltwater-drainage pathways in northern central Europe: Insights from 2D numerical flood simulation. *Quatern. Sci. Rev.*, **209**, 82–99.

Launder, B.E. and **Rodi, W.** (1983) The turbulent wall jet measurements and modeling. *Annu. Rev. Fluid Mech.*, **15**, 429–459.

Le Heron, D.P., **Sutcliffe, O.**, **Bourgig, K.**, **Craig, J.**, **Visentin, C.** and **Whittington, R.** (2004) Sedimentary architecture of Upper Ordovician tunnel valleys, Gargaf Arch, Libya: implications for the genesis of a hydrocarbon reservoir. *GeoArabia*, **9**, 137–160.

Le Heron, D.P., **Craig, J.**, **Sutcliffe, O.E.** and **Whittington, R.** (2006) Late Ordovician glaciogenic reservoir heterogeneity: an example from the Murzuq Basin, Libya. *Mar. Petrol. Geol.*, **23**, 655–677.

Le Heron, D.P., **Craig, J.** and **Etienne, J.L.** (2009) Ancient glaciations and hydrocarbon accumulations in North Africa and the Middle East. *Earth.-Sci. Rev.*, **93**, 47–76.

Le Heron, D.P., **Armstrong, H.A.**, **Wilson, C.**, **Howard, J.P.** and **Gindre, L.** (2010) Glaciation and deglaciation of the Libyan Desert: the Late Ordovician record. *Sed. Geol.*, **223**, 100–125.

Le Heron, D.P., **Meinhold, G.**, **Page, A.** and **Whitham, A.** (2013) Did lingering ice sheets moderate anoxia in the Early Palaeozoic of Libya? *J. Geol. Soc.*, **170**, 327–339.

Le Heron, D.P., **Busfield, M.E.** and **Collins, A.S.** (2014) Bolla Bollana boulder beds: A Neoproterozoic trough mouth fan in South Australia? *Sedimentology*, **61**, 978–995.

Le Heron, D.P., **Meinhold, G.**, **Elgadry, M.**, **Abutarruma, Y.** and **Boote, D.** (2015) Early Palaeozoic evolution of Libya: perspectives from Jabal Eghei with implications for hydrocarbon exploration in Al Kufrah Basin. *Basin Res.*, **27**, 60–83.

Lechte, M.A., **Wallace, M.W.** and **Hood, A.V.S.** and **Planavsky, N.** (2018) Cryogenian iron formations in the glaciogenic Kingston Peak Formation, California. *Precambrian Res.*, **310**, 443–462.

Lee, J.R., **Wakefield, O.J.**, **Phillips, E.** and **Hughes, L.** (2015) Sedimentary and structural evolution of a relict subglacial to subaerial drainage system and its hydrogeological implications: an example from Anglesey, north Wales, UK. *Quatern. Sci. Rev.*, **109**, 88–110.

Leszczynska, K., **Boreham, S.** and **Gibbard, P. L.** (2017) Middle Pleistocene ice-marginal sedimentation in the transitional zone between the constrained and unconstrained ice-sheet margin, East Anglia, England. *Boreas*, **46**, 697–724.

Leszczynska, K., **Boreham, S.** and **Gibbard, P. L.** (2018) Middle Pleistocene ice-marginal sedimentation at a constrained ice-sheet margin, East Anglia, UK. *Boreas*, **47**, 1118–1143.

Lønne, I. (1995) Sedimentary facies and depositional architecture of ice-contact glaciomarine systems. *Sed. Geol.*, **98**, 13–43.

Lønne, I. (1997) Facies characteristics of a proglacial turbiditic sand-lobe at Svalbard. *Sed. Geol.*, **109**, 13–35.

Lønne, I. (2001) Dynamics of marine glacier termini read from moraine architecture. *Geology*, **29**, 199–202.

Macdonald, R.G., **Alexander, J.**, **Bacon, J.C.** and **Cooker, M.J.** (2009) Flow patterns, sedimentation and deposit architecture under a hydraulic jump on a non-eroding bed: defining hydraulic-jump unit bars. *Sedimentology*, **56**, 1346–1367.

Macdonald, R.G., **Alexander, J.**, **Bacon, J.C.** and **Cooker, M.J.** (2013) Variations in the architecture of hydraulic-jump bar complexes on non-eroding beds. *Sedimentology*, **60**, 1291–1312.

Mangerud, J., **Jakobsson, M.**, **Alexanderson, H.**, **Astakhov, V.**, **Clarke, G.K.**, **Henriksen, M.**, **Hjort, C.**, **Krinner, G.**, **Lunkka, J.-P.**, **Möller, P.**, **Murray, A.**, **Nikolskaya, O.**, **Saarnisto, M.** and **Svendsen, J.I.** (2004) Ice-dammed lakes and rerouting of the drainage of northern Eurasia during the Last Glaciation. *Quatern. Sci. Rev.*, **23**, 1313–1332.

Margold, M., **Jansen, J.D.**, **Codilean, A.T.**, **Preusser, F.**, **Gurinov, A.L.**, **Fujioka, T.** and **Fink, D.** (2018) Repeated megafloods from glacial Lake Vitim, Siberia, to the Arctic Ocean over the past 60,000 years. *Quatern. Sci. Rev.*, **187**, 41–61.

Marren, P.M. (2005) Magnitude and frequency in proglacial rivers: a geomorphological and sedimentological perspective. *Earth-Sci. Rev.*, **70**, 203–251.

Martin, J.R., **Redfern, J.** and **Williams, B.P.J.** (2012) Evidence for multiple ice centres during the late Palaeozoic ice age in Oman: outcrop sedimentology and provenance of the Late Carboniferous–Early Permian Al Khlata Formation. *Geol. Soc., London, Spec. Pub.*, **368**(1), 229–256.

Martinius, A.W. and **Van den Berg, J.H.** (2011) *Atlas of Sedimentary Structures In Estuarine And Tidally-Influenced River Deposits Of The Rhine-Meuse-Scheldt System: Their Application To The Interpretation Of Analogous Outcrop And Subsurface Depositional Systems*. EAGE Publications, Houten, 298 pp.

Massari, F. (1996) Upper-flow-regime stratification types on steep-face, coarse-grained, Gilbert-type progradational wedges (Pleistocene, southern Italy). *J. Sed. Res.*, **66**, 364–375.

Massari, F. (2017) Supercritical-flow structures (backset-bedded sets and sediment waves) on high-gradient clinoform systems influenced by shallow-marine hydrodynamics. *Sed. Geol.*, **360**, 73–95.

Mastbergen, D.R. and **Van Den Berg, J.H.** (2003) Breaching in fine sands and the generation of sustained turbidity currents in submarine canyons. *Sedimentology*, **50**, 625–637.

Middleton, G.V. (1965) Antidune cross-bedding in a large flume. *J. Sed. Petrol.*, **35**, 922–927.

Montañez, I. P. and **Poulsen, C. J.** (2013) The late paleozoic ice age: An evolving paradigm. *Annu. Rev. Earth Planet. Sci.*, **41**, 629–656.

Moreau, J. and **Joubert, J.B.** (2016) Glacial sedimentology interpretation from borehole image log: Example from the Late Ordovician deposits, Murzuq Basin. *Interpretation*, **4**, 1–16.

Mulder, T. and **Alexander, J.** (2001) The physical character of subaqueous sedimentary density flows and their deposits. *Sedimentology*, **48**, 269–299.

Muto, T., **Yamagishi, C.**, **Sekiguchi, T.**, **Yokokawa, M.** and **Parker, G.** (2012) The hydraulic autogenesis of distinct cyclicity in delta foreset bedding: flume experiments. *J. Sed. Res.*, **82**, 545–558.

Mutti, E. and **Normark, W.R.** (1987) Comparing examples of modern and ancient turbidite systems: problems and concepts. In: *Marine Clastic Sedimentology* (Eds Leggett, J.K. and Zuffa, G.G.), pp. 1–38. Springer, Dordrecht.

Nehyba, S., **Hanáček, M.**, **Engel, Z.** and **Stachoň, Z.** (2017) Rise and fall of a small ice-dammed lake-Role of deglaciation processes and morphology. *Geomorphology*, **295**, 662–679.

Nemec, W. (1990) Aspects of sediment movement on steep delta slopes. In: *Coarse-Grained Deltas* (Eds Colella, A. and Prior, B.D.), *Int. Assoc. Sed. Spec. Publ.*, **10**, 29–73.

Nielsen, L.H., **Johannessen, P.N.** and **Surlyk, F.** (1988) A Late Pleistocene coarse-grained spit-platform sequence in northern Jylland, Denmark. *Sedimentology*, **35**, 915–937.

Normandeau, A., **Lajeunesse, P.**, **Poiré, A.G.** and **Francus, P.** (2016) Morphological expression of bedforms formed by supercritical sediment density flows on four fjord-lake deltas of the south-eastern Canadian Shield (Eastern Canada). *Sedimentology*, **63**, 2106–2129.

Normandeau, A., **Dietrich, P.**, **Lajeunesse, P.**, **St-Onge, G.**, **Ghienne, J.F.**, **Duchesne, M.J.** and **Francus, P.** (2017) Timing and controls on the delivery of coarse sediment to deltas and submarine fans on a formerly glaciated coast and shelf. *GSA Bull.*, **129**, 1424–1441.

Okazaki, H., **Isaji, S.** and **Kurozumi, T.** (2020) Sedimentary facies related to supercritical-flow bedforms in foreset slopes of a Gilbert-type delta (middle Pleistocene, Central Japan). *Sed. Geol.*, **399**, 105613.

Onishi, Y., **Takii-Kawakami, K.**, **Abe, H.** and **Ishihara, Y.** (2018) Facies distribution in sediment-gravity-flow deposits constructing sediment waves: an outcrop example of forearc basin fills, Neogene Aoshima Formation, southwest Japan. *J. Sed. Res.*, **88**, 260–275.

Ono, K. and **Plink-Björklund, P.** (2018) Froude supercritical flow bedforms in deepwater slope channels? Field examples in conglomerates, sandstones and fine-grained deposits. *Sedimentology*, **65**, 639–669.

Ono, K., **Plink-Björklund, P.**, **Eggenhuisen, J.T.** and **Cartigny, M.J.B.** (2021) Froude supercritical flow processes and sedimentary structures: New insights from experiments with a wide range of grain sizes. *Sedimentology*, **68**, 1328–1357.

Panin, A.V., **Astakhov, V.I.**, **Lotsari, E.**, **Komatsu, G.**, **Lang, J.** and **Winsemann, J.** (2020) Middle and Late Quaternary glacial lake-outburst floods, drainage diversions and reorganization of fluvial systems in northwestern Eurasia. *Earth-Sci. Rev.*, **201**, 103069.

Paola, C., **Wiele, S.M.** and **Reinhart, M.A.** (1989) Upper-regime parallel lamination as the result of turbulent sediment transport and low-amplitude bed forms. *Sedimentology*, **36**, 47–59.

Pisarska-Jamroży, M. and **Zieliński, T.** (2014) Pleistocene sandur rhythms, cycles and megacycles: Interpretation of depositional scenarios and palaeoenvironmental conditions. *Boreas*, **43**, 330–348.

Plink-Björklund, P. and **Ronnert, L.** (1999) Depositional processes and internal architecture of late Weichselian ice margin submarine fan and delta settings, Swedish west coast. *Sedimentology*, **46**, 215–234.

Postma, G. and **Cartigny, M.J.B.** (2014) Supercritical and subcritical turbidity currents and their deposits – A synthesis. *Geology*, **42**, 987–990.

Postma, G. and **Kleverlaan, K.** (2018) Supercritical flows and their control on the architecture and facies of small-radius sand-rich fan lobes. *Sed. Geol.*, **364**, 53–70.

Postma, G., **Nemec, W.** and **Kleinspehn, K.L.** (1988) Large floating clasts in turbidites: a mechanism for their emplacement. *Sed. Geol.*, **58**, 47–61.

Postma, G., **Cartigny, M.J.B.** and **Kleverlaan, K.** (2009) Structureless, coarse-tail graded Bouma Ta formed by internal hydraulic jump of the turbidity current? *Sed. Geol.*, **219**, 1–6.

Postma, G., **Kleverlaan, K.** and **Cartigny, M.J.B.** (2014) Recognition of cyclic steps in sandy and gravelly turbidite sequences, and consequences for the Bouma facies model. *Sedimentology*, **61**, 2268–2290.

Postma, G., **Hoyal, D.C.**, **Demko, T.**, **Fedele, J.J.**, **Lang, J.**, **Abreu, V.** and **Pederson, K.H.** (2021) Reconstruction of supercritical flow bedform morphodynamics in the channel-lobe transition zone of a deep-water delta (Sant Llorenç del Munt, N. Spain, Eocene). *Sedimentology*, **68**, 1674–1697.

Powell, R.D. (1990) Glacimarine processes at grounding-line fans and their growth to ice-contact deltas. *Geol. Soc., London, Spec. Pub.*, **53**(1), 53–73.

Røe, S.-L. (1987) Cross-strata and bedforms of probable transitional dune to upper-stage plane-bed origin from a Late Precambrian fluvial sandstone, northern Norway. *Sedimentology*, **34**, 89–101.

Rubi, R., **Rohais, S.**, **Bourquin, S.**, **Moretti, I.** and **Desaubliaux, G.** (2018) Processes and typology in Gilbert-type delta bottomset deposits based on outcrop examples in the Corinth Rift. *Mar. Petrol. Geol.*, **92**, 193–212.

Russell, H.A.J. and **Arnott, R.W.C.** (2003) Hydraulic jump and hyperconcentrated-flow deposits of a glacigenic subaqueous fan: Oak Ridges Moraine, Southern Ontario, Canada. *J. Sed. Res.*, **73**, 887–905.

Russell, H.A.J. and **Knudsen, Ó.** (2002) The effects of glacier-outburst flood flow dynamics on ice-contact deposits: November 1996 jökulhlaup, Skeiðarársandur, Iceland. In: *Flood and Megaflood Processes and Deposits: Recent and Ancient Examples* (Eds Martini, I.P., Baker, V.R. and Garzón, G.), *IAS Spec. Publ.*, **32**, 67–83.

Russell, H.A.J., **Arnott, R.W.C.** and **Sharpe, D.R.** (2003) Evidence for rapid sedimentation in a tunnel channel, Oak Ridges Moraine, southern Ontario, Canada. *Sed. Geol.*, **160**, 33–55.

Russell, H.A.J., **Sharpe, D.R.** and **Bajk, A. F.** (2007) Sedimentary signatures of the Waterloo Moraine, Ontario, Canada. In: *Glacial Processes and Products* (Eds Hambrey, M., Christoffersen, P., Glasser, N. and Hubbard, B.), *Int. Assoc. Sed. Spec. Publ.*, **39**, 85–108.

Rust, B.R. and **Romanelli, R.** (1975) Late Quaternary subaqueous outwash deposits near Ottawa, Canada. In: *Glaciofluvial and Glaciolacustrine Sedimentation* (Eds Jopling, A.V. and McDonald, B.C.), *SEPM Spec. Publ.*, **23**, 177–192.

Saunderson, H.C. and **Lockett, F.P.J.** (1983) Flume experiments on bedforms and structures at the dune-plane bed transition. In: *Modern and Ancient Fluvial Systems* (Eds Collinson, J. D. and Lewin, L.), *Spec. Pub. Int. Ass. Sediment*, **6**, 49–58.

Selim, S.S. (2019) Sedimentological model, architecture, and evolution of a shallow-water Gilbert-type delta from the Lower Miocene, Red Sea Rift, Egypt. *Int. Geol. Rev.*, https://doi.org/10.1080/00206814.2019.1686659.

Sequeiros, O.E. (2012) Estimating turbidity current conditions from channel morphology: A Froude number approach. *J. Geophys. Res.*, **117**, 1–19.

Slomka, J.M. and **Hartman, G.M.D.** (2019) Sedimentary architecture of a glaciolacustrine braidplain delta: proxy evidence of a pre-Middle Wisconsinan glaciation

(Grimshaw gravels, Interior Plains, Canada). *Boreas*, **48**, 215–235.

Slootman, A. and **Cartigny, M.J.B.** (2019) Cyclic steps: Review and aggradation-based classification. *Earth-Sci. Rev.*, **201**, 102949.

Slootman, A., **Cartigny, M.J.B.**, **Moscariello, A.**, **Chiaradia, M.** and **de Boer, P.L.** (2016) Quantification of tsunami-induced flows on a Mediterranean carbonate ramp reveals catastrophic evolution. *Earth Planet. Sci. Lett.*, **444**, 192–204.

Slootman, A., **Simpson, G.**, **Castelltort, S.** and **de Boer, P.L.** (2018) Geological record of marine tsunami backwash: The role of the hydraulic jump. *Deposit. Rec.*, **4**, 59–77.

Slootman, A., **De Boer, P.L.**, **Cartigny, M.J.B.**, **Samankassou, E.** and **Moscariello, A.** (2019) Evolution of a carbonate delta generated by gateway-funnelling of episodic currents. *Sedimentology*, **66**, 1302–1340.

Sohn, Y.K. (1997) On traction-carpet sedimentation. *J. Sed. Res.*, **67**, 502–509.

Spence, G.H., **Le Heron, D.P.** and **Fairchild, I.J.** (2016) Sedimentological perspectives on climatic, atmospheric and environmental change in the Neoproterozoic Era. *Sedimentology*, **63**, 253–306.

Stacey, C.D. and **Hill, P.R.** (2016) Cyclic steps on a glacifluvial delta, Howe Sound, British Columbia. *Geol. Soc., London, Mem.*, **46**(1), 93–94.

Stacey, C.D., **Hill, P.R.**, **Talling, P.J.**, **Enkin, R.J.**, **Hughes Clarke, J.** and **Lintern, D.G.** (2019) How turbidity current frequency and character varies down a fjord-delta system: Combining direct monitoring, deposits and seismic data. *Sedimentology*, **66**, 1–31.

Steinmetz, D., **Winsemann, J.**, **Brandes, C.**, **Siemon, B.**, **Ullmann, A.**, **Wiederhold, H.** and **Meyer, U.** (2015) Towards an improved geological interpretation of airborne electromagnetic data: a case study from the Cuxhaven tunnel valley and its Neogene host sediments (northwest Germany). *Neth. J. Geosci.*, **94**, 201–227.

Strong, N. and **Paola, C.** (2008) Valleys that never were: time versus stratigraphic surfaces. *J. Sed. Res.*, **78**, 579–593.

Symons, W.O., **Sumner, E.J.**, **Talling, P.J.**, **Cartigny, M.J.B.** and **Clare, M.A.** (2016) Large-scale sediment waves and scours on the modern seafloor and their implications for the prevalence of supercritical flows. *Mar. Geol.*, **371**, 130–148.

Talling, P.J., **Masson, D.G.**, **Sumner, E.J.** and **Malgesini, G.** (2012) Subaqueous sediment density flows: Depositional processes and deposit types. *Sedimentology*, **59**, 1937–2003.

Van den Berg, J.H. and **Van Gelder, A.** (1998) Discussion: Flow and sediment transport over large subaqueous dunes: Fraser River, Canada. *Sedimentology*, **45**, 217–219.

Van den Berg, J.H. and **Lang, J.** (this issue) Submarine cyclic step deposits of a Miocene volcanic island, Cuatro Calas, SE Spain. *Sedimentology*.

Van den Berg, J.H. and **Van Gelder, A.** (1993) A new bedform stability diagram, with emphasis on the transition of ripples to plane bed in flows over fine sand and silt. In: *Alluvial Sedimentation* (Eds Marzo, M. and Puigdefabregas, C.), *Int. Assoc. Sed. Spec. Publ.*, **17**, 11–21.

Vaucher, R., **Pittet, B.**, **Humbert, T.** and **Ferry, S.** (2018) Large-scale bedforms induced by supercritical flows and wave–wave interference in the intertidal zone (Cap Ferret, France). *Geo-Mar. Lett.*, **38**, 287–305.

Vendettuoli, D., **Clare, M.A.**, **Clarke, J.H.**, **Vellinga, A.**, **Hizzet, J.**, **Hage, S.**, **Cartigny, M.J.B.**, **Talling, P.J.**, **Waltham, D.**, **Hubbard, S.M.**, **Stacey, C.** and **Lintern, D.G.** (2019) Daily bathymetric surveys document how stratigraphy is built and its extreme incompleteness in submarine channels. *Earth Planet. Sci. Lett.*, **515**, 231–247.

Vellinga, A.J., **Cartigny, M.J.B.**, **Eggenhuisen, J.T.** and **Hansen, E.W.** (2018) Morphodynamics and depositional signature of low-aggradation cyclic steps: New insights from a depth-resolved numerical model. *Sedimentology*, **65**, 540–560.

Ventra, D., **Cartigny, M.J.B.**, **Bijkerk, J.F.** and **Acikalin, S.** (2015) Supercritical-flow structures on a Late Carboniferous delta front: Sedimentologic and paleoclimatic significance. *Geology*, **43**, 731–734.

Vesely, F., **Trzaskos, B.**, **Kipper, F.**, **Assine, M.L.** and **Souza, P.A.** (2015) Sedimentary record of a fluctuating ice margin from the Pennsylvanian of western Gondwana: Paraná Basin, southern Brazil. *Sed. Geol.*, **326**, 45–63.

Virtasalo, J.J., **Schröder, J.F.**, **Luoma, S.**, **Majaniemi, J.**, **Mursu, J.** and **Scholten, J.** (2019) Submarine groundwater discharge site in the First Salpausselkä ice-marginal formation, south Finland. *Solid Earth*, **10**, 405–423.

Wang, J. and **Plink-Björklund, P.** (2020) Variable-discharge-river macroforms in the Sunnyside Delta Interval of the Eocene Green River Formation, Uinta Basin, USA. *Sedimentology*, **67**, 1914–1950.

West, L.M., **Perillo, M.M.**, **Olariu, C.** and **Steel, R.J.** (2019) Multi-event organization of deepwater sediments into bedforms: Long-lived, large-scale antidunes preserved in deepwater slopes. *Geology*, **47**, 391–394.

Winsemann, J., **Asprion, U.** and **Meyer, T.** (2004) Sequence analysis of early Saalian glacial lake deposits (NW Germany): evidence of local ice margin retreat and associated calving processes. *Sed. Geol.*, **165**, 223–251.

Winsemann, J., **Asprion, U.** and **Meyer, T.** (2007a) Lake-level control on ice-margin subaqueous fans, glacial Lake Rinteln. In: *Glacial Processes and Products* (Eds Hambrey, M., Christoffersen, P. Glasser, N. and Hubbard, B.), *Int. Assoc. Sed. Spec. Publ.*, **39**, 121–148.

Winsemann, J., **Asprion, U.**, **Meyer, T.** and **Schramm, C.** (2007b) Facies characteristics of Middle Pleistocene (Saalian) ice-margin subaqueous fan and delta deposits, glacial Lake Leine, NW Germany. *Sed. Geol.*, **193**, 105–129.

Winsemann, J., **Hornung, J.J.**, **Meinsen, J.**, **Asprion, U.**, **Polom, U.**, **Brandes, C.**, **Bußmann, M.** and **Weber, C.** (2009) Anatomy of a subaqueous ice-contact fan and delta complex, Middle Pleistocene, NW Germany. *Sedimentology*, **56**, 1041–1076.

Winsemann, J., **Brandes, C.** and **Polom, U.** (2011) Response of a proglacial delta to rapid high-amplitude lake-level change: an integration of outcrop data and high-resolution shear wave seismic. *Basin Res.*, **23**, 22–52.

Winsemann, J., **Alho, P.**, **Laamanen, L.**, **Goseberg, N.**, **Lang, J.** and **Klostermann, J.** (2016) Flow dynamics, sedimentation and erosion of glacial lake outburst floods along the Middle Pleistocene Scandinavian Ice Sheet (northern central Europe). *Boreas*, **45**, 260–283.

Winsemann, J., **Lang, J.**, **Polom, U.**, **Loewer, M.**, **Igel, J.**, **Pollok, L.** and **Brandes, C.** (2018) Ice-marginal forced-regressive deltas in glacial lake basins: geomorphology, facies variability and large-scale depositional architecture. *Boreas*, **47**, 973–1002.

Yagishita, K. (1994) Antidunes and traction-carpet deposits in deep-water channel sandstones, Cretaceous, British Columbia, Canada. *J. Sed. Res.*, **64**, 34–41.

Zhong, G., **Cartigny, M.J.B.**, **Kuang, Z.** and **Wang, L.** (2015) Cyclic steps along the South Taiwan Shoal and West Penghu submarine canyons on the northeastern continental slope of the South China Sea. *GSA Bull.*, **127**, 804–824.

Zielinski, T. and **van Loon, A.J.** (2002) Present-day sandurs are not representative of the geological record. *Sed. Geol.*, **152**, 1–5.

Zielinski, T. and **van Loon, A.J.** (2003) Pleistocene sandur deposits represent braidplains, not alluvial fans. *Boreas*, **32**, 590–611.

Manuscript received 28 May 2019; revision 7 June 2020; revision accepted 16 June 2020

Supporting Information

Additional information may be found in the online version of this article:

Table S1. Settings, locations and references of the outcrop examples.